Energy Landscapes, Pathways and Dynamics: From Atomic to Mesoscopic Systems

Objective: to exploit stationary points (minima and transition states) of the PES as a computational framework (*J. Phys. Chem. B*, **110**, 20765, 2006):

- Basin-hopping for global optimisation (*J. Phys. Chem. A*, **101**, 5111 1997)
- Basin-sampling for global thermodynamics (*J. Chem. Phys.*, **124**, 044102, 2006)
- Discrete path sampling for global kinetics (*Mol. Phys.*, **100**, 3285, 2002)

For small molecules (left), all the relevant stationary points and pathways can be located. Larger systems (right) require appropriate sampling.

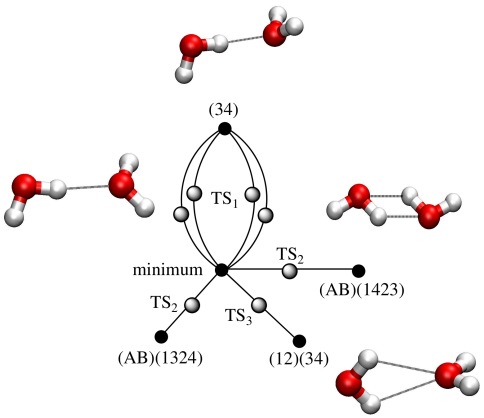

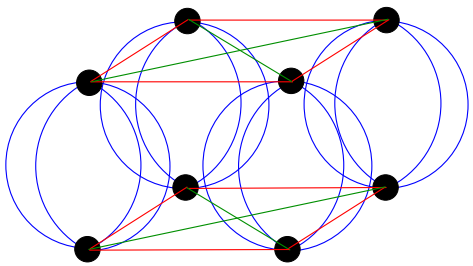

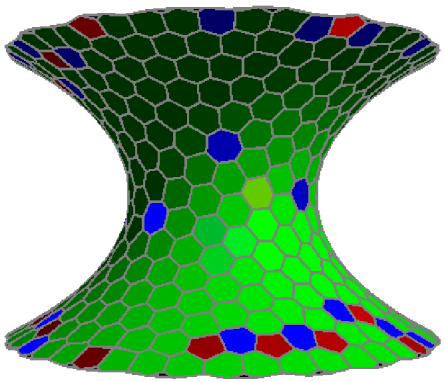

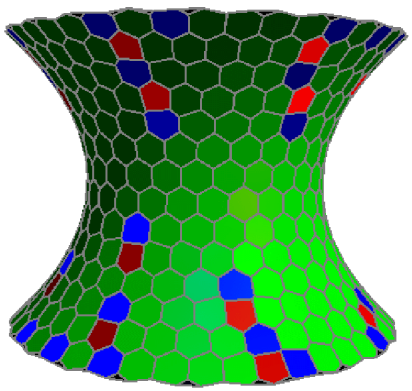

Tunneling in $(H_2O)_2$

The largest number of versions connected by feasible rearrangements is 8, and the largest MS group has order 16 (*J. Chem. Phys.*, **120**, 5993, 2004).

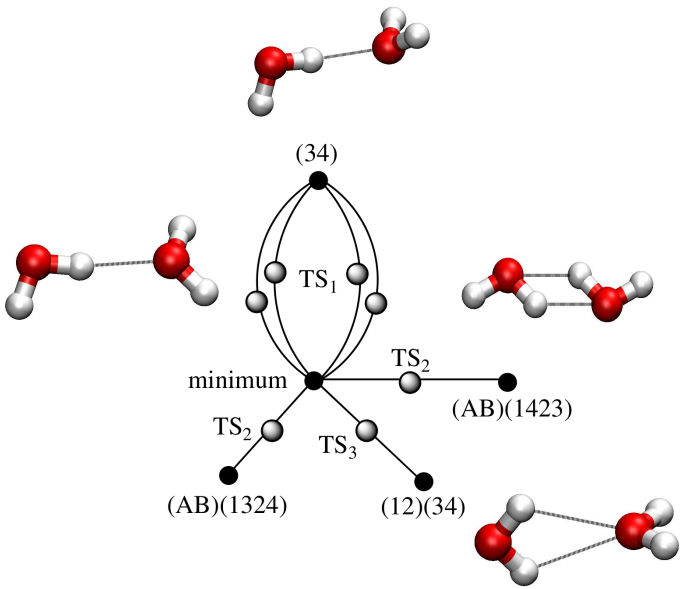

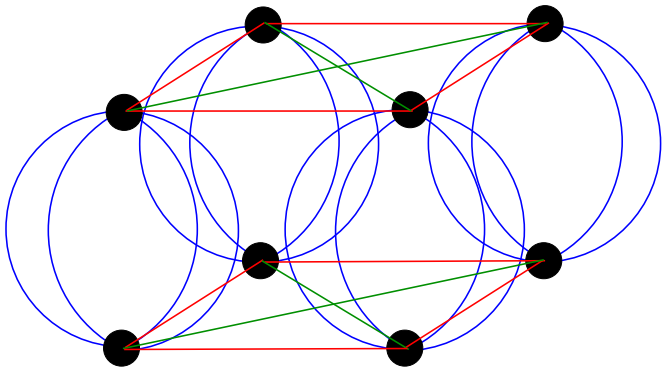

Acceptor tunneling produces the biggest tunneling splitting via a 'methylamine-type' process resulting in doublet splittings and an MS group of order 4. The next-largest splitting comes from donor-acceptor interchange producing an MS group of order 16 and a doublet of triplets.

Bifurcation (donor) tunneling simply causes a shift in the energy levels.

Tunneling in $(H_2O)_3$ (*Chem. Rev.*, **103**, 2533, 2003)

Far-infrared vibration-rotation tunneling spectroscopy probes large amplitude motion (Saykally and coworkers). Resolution: $1\,\mathrm{MHz}$ ($3 \times 10^{-5}\,\mathrm{cm}^{-1}$).

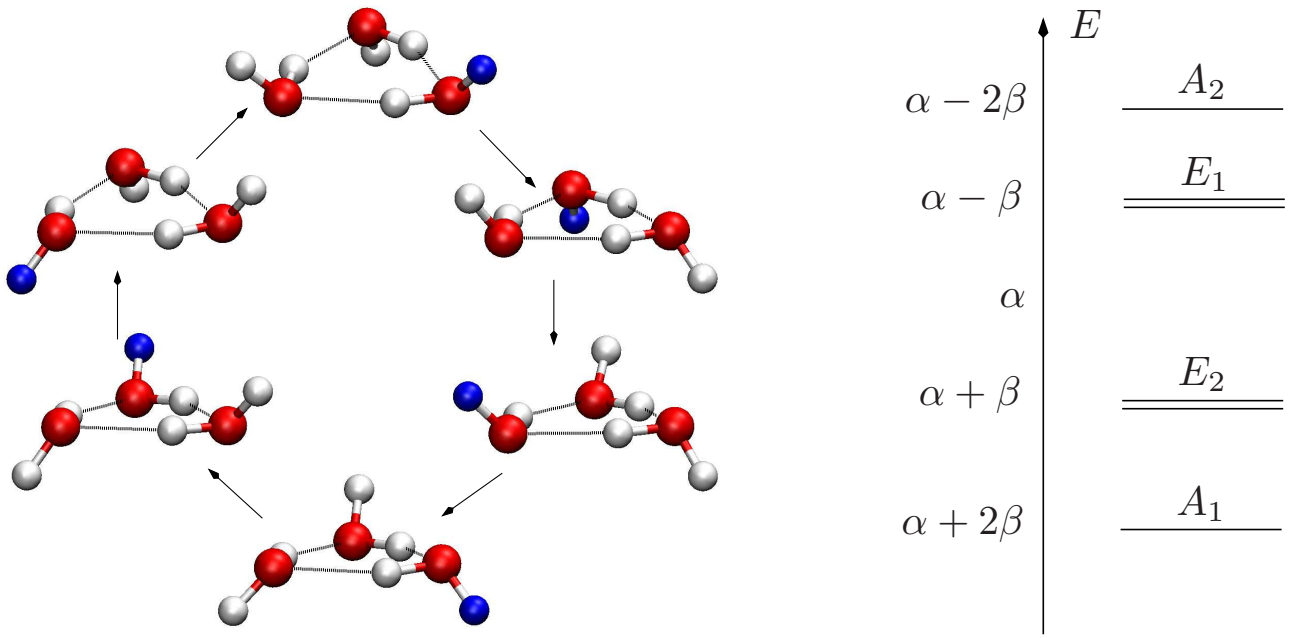

For $(H_2O)_3$ there are two 'feasible' rearrangement mechanisms.

The facile 'flip' causes vibrational averaging of the rotational constants with splittings of order $10\,\mathrm{cm}^{-1}$ and links permutational isomers in sets of six, producing a splitting pattern analogous to the π system of benzene and an MS group isomorphic to C_{3h} (*J. Am. Chem. Soc.*, **115**, 11180, 1993).

Bifurcation tunneling links versions in pairs. When combined with the flip 48 versions are connected, which can be partitioned into eight sets of six.

Depending on the level of theory, a bifurcation may be accompanied by zero, one or two flips of the neighbouring water molecules.

There are actually six ways of combining the bifurcation with these flips to give degenerate rearrangements, and two distinct splitting patterns:

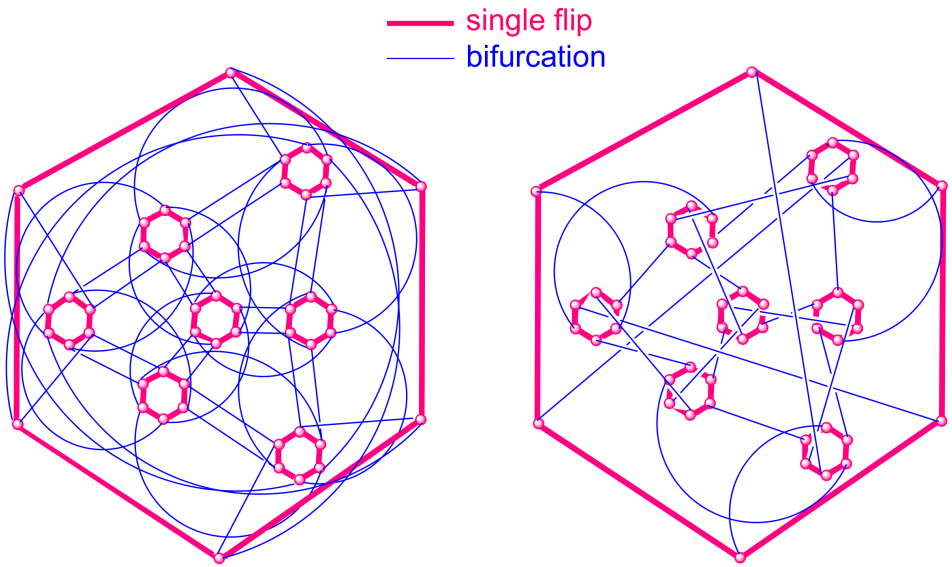

Group A

bifurcation + no flip / single flip

Group B

bifurcation + double flip

Only one pattern has entirely regular quartets and the corresponding generators all contain E^*, in agreement with analysis of Coriolis splittings.

The quartet splittings are of order $0.01\,\mathrm{cm}^{-1}$; spectra have now been successfully assigned for various isotopomers (*J. Chem. Phys.*, **117**, 8823, 2002).

The tunneling matrix elements for the flip and bifurcation, β_{f} and β_{b}, have been estimated from the geometrical pathways using a semiclassical approach.

A vibrationally adiabatic effective potential was defined as

$$V_{\mathrm{a}}(s) = V_{\mathrm{SD}}(s) + V_{\mathrm{vib}}(s), \tag{1}$$

where $V_{\mathrm{SD}}(s)$ is the potential energy along the steepest-descent pathways (calculated at the MP2/aug-cc-pVTZ level) as a function of the path length, s, and $V_{\mathrm{vib}}(s)$ is the sum of zero-point energies for the other modes.

The WKB approach was then applied to $V_{\mathrm{a}}(s)$.

Tunneling matrix elements were calculated as $\beta = \hbar\nu \exp(-\theta)$, where ν is the vibrational frequency corresponding to the given rearrangement and

$$\theta = \frac{1}{\hbar} \int_{s_0}^{s_1} \sqrt{2(V_{\mathrm{a}}(s) - E)}\, ds, \tag{1}$$

where the integration limits are defined by $V_{\mathrm{a}}(s_0) = V_{\mathrm{a}}(s_1) = E$, and E is the zero-point energy for the reaction mode.

The observed tunnelling splittings correspond to $2\beta_{\mathrm{f}}$ for the flip and $4\beta_{\mathrm{b}}/3$ for the bifurcation, giving values in cm^{-1} (*J. Chem. Phys.*, **123**, 044302, 2005)

	calculated	experiment
Flip		
$(H_2O)_3$	37.93	43.52
$(D_2O)_3$	30.84	20.54
Bifurcation		
$(H_2O)_3$	6.50×10^{-3}	9.63×10^{-3}
$(D_2O)_3$	2.54×10^{-5}	1.66×10^{-4}

Tunneling in $(H_2O)_5$ (*J. Chem. Phys.*, **105**, 6957, 1996)

$\mathcal{G}(320)$	1	1	5	5	5	5	5	5	16	16	16	16	16	16	16	16	1	1	5	5	5	5	5	5	16	16	16	16	16	16	16	16
A_1^+	1	1	1	1	1	1	1	1	1	1	1	1	1	1	1	1	1	1	1	1	1	1	1	1	1	1	1	1	1	1	1	1
A_2^+	1	-1	-1	1	1	-1	-1	1	1	-1	1	-1	1	-1	-1	1	1	-1	-1	1	1	-1	-1	1	1	-1	1	-1	1	-1	-1	1
E_1^+	2	2	2	2	2	2	2	2	ϕ	ϕ	$-\phi$	$-\phi$	$-\phi$	$-\phi$	ϕ	ϕ	2	2	2	2	2	2	2	2	ϕ	ϕ	$-\phi$	$-\phi$	$-\phi$	$-\phi$	ϕ	ϕ
E_2^+	2	2	2	2	2	2	2	2	$-\phi$	$-\phi$	ϕ	ϕ	ϕ	ϕ	$-\phi$	$-\phi$	2	2	2	2	2	2	2	2	$-\phi$	$-\phi$	ϕ	ϕ	ϕ	ϕ	$-\phi$	$-\phi$
E_3^+	2	-2	-2	2	2	-2	-2	2	ϕ	$-\phi$	$-\phi$	ϕ	$-\phi$	ϕ	$-\phi$	ϕ	2	-2	-2	2	2	-2	-2	2	ϕ	$-\phi$	$-\phi$	ϕ	$-\phi$	ϕ	$-\phi$	ϕ
E_4^+	2	-2	-2	2	2	-2	-2	2	$-\phi$	ϕ	ϕ	$-\phi$	ϕ	$-\phi$	ϕ	$-\phi$	2	-2	-2	2	2	-2	-2	2	$-\phi$	ϕ	ϕ	$-\phi$	ϕ	$-\phi$	ϕ	$-\phi$
H_1^+	5	5	1	1	-3	1	-3	1	0	0	0	0	0	0	0	0	5	5	1	1	-3	1	-3	1	0	0	0	0	0	0	0	0
H_2^+	5	5	1	-3	1	-3	1	1	0	0	0	0	0	0	0	0	5	5	1	-3	1	-3	1	1	0	0	0	0	0	0	0	0
H_3^+	5	-5	-1	1	-3	-1	3	1	0	0	0	0	0	0	0	0	5	-5	-1	1	-3	-1	3	1	0	0	0	0	0	0	0	0
H_4^+	5	-5	-1	-3	1	3	-1	1	0	0	0	0	0	0	0	0	5	-5	-1	-3	1	3	-1	1	0	0	0	0	0	0	0	0
H_5^+	5	5	-3	1	1	1	1	-3	0	0	0	0	0	0	0	0	5	5	-3	1	1	1	1	-3	0	0	0	0	0	0	0	0
H_6^+	5	-5	3	1	1	-1	-1	-3	0	0	0	0	0	0	0	0	5	-5	3	1	1	-1	-1	-3	0	0	0	0	0	0	0	0
A_1^-	1	1	1	1	1	1	1	1	1	1	1	1	1	1	1	1	-1	-1	-1	-1	-1	-1	-1	-1	-1	-1	-1	-1	-1	-1	-1	-1
A_2^-	1	-1	-1	1	1	-1	-1	1	1	-1	1	-1	1	-1	-1	1	-1	1	1	-1	-1	1	1	-1	-1	1	-1	1	-1	1	1	-1
E_1^-	2	2	2	2	2	2	2	2	ϕ	ϕ	$-\phi$	$-\phi$	$-\phi$	$-\phi$	ϕ	ϕ	-2	-2	-2	-2	-2	-2	-2	-2	$-\phi$	$-\phi$	ϕ	ϕ	ϕ	ϕ	$-\phi$	$-\phi$
E_2^-	2	2	2	2	2	2	2	2	$-\phi$	$-\phi$	ϕ	ϕ	ϕ	ϕ	$-\phi$	$-\phi$	-2	-2	-2	-2	-2	-2	-2	-2	ϕ	ϕ	$-\phi$	$-\phi$	$-\phi$	$-\phi$	ϕ	ϕ
E_3^-	2	-2	-2	2	2	-2	-2	2	ϕ	$-\phi$	$-\phi$	ϕ	$-\phi$	ϕ	$-\phi$	ϕ	-2	2	2	-2	-2	2	2	-2	$-\phi$	ϕ	ϕ	$-\phi$	ϕ	$-\phi$	ϕ	$-\phi$
E_4^-	2	-2	-2	2	2	-2	-2	2	$-\phi$	ϕ	ϕ	$-\phi$	ϕ	$-\phi$	ϕ	$-\phi$	-2	2	2	-2	-2	2	2	-2	ϕ	$-\phi$	$-\phi$	ϕ	$-\phi$	ϕ	$-\phi$	ϕ
H_1^-	5	5	1	1	-3	1	-3	1	0	0	0	0	0	0	0	0	-5	-5	-1	-1	3	-1	3	-1	0	0	0	0	0	0	0	0
H_2^-	5	5	1	-3	1	-3	1	1	0	0	0	0	0	0	0	0	-5	-5	-1	3	-1	3	-1	-1	0	0	0	0	0	0	0	0
H_3^-	5	-5	-1	1	-3	-1	3	1	0	0	0	0	0	0	0	0	-5	5	1	-1	3	1	-3	-1	0	0	0	0	0	0	0	0
H_4^-	5	-5	-1	-3	1	3	-1	1	0	0	0	0	0	0	0	0	-5	5	1	3	-1	-3	1	-1	0	0	0	0	0	0	0	0
H_5^-	5	5	-3	1	1	1	1	-3	0	0	0	0	0	0	0	0	-5	-5	3	-1	-1	-1	-1	3	0	0	0	0	0	0	0	0
H_6^-	5	-5	3	1	1	-1	-1	-3	0	0	0	0	0	0	0	0	-5	5	-3	-1	-1	1	1	3	0	0	0	0	0	0	0	0

Feasible flip and bifurcation mechanisms also exist for $(H_2O)_5$, giving a molecular symmetry group of order 320. $\phi = (\sqrt{5}+1)/2$ and $\phi = 1/\phi = \phi - 1$.

Tunneling splittings have now been assigned experimentally using $\mathcal{G}(320)$.

Tunnelling in $(H_2O)_4$ (*J. Chem. Phys.*, **106**, 7193, 1997)

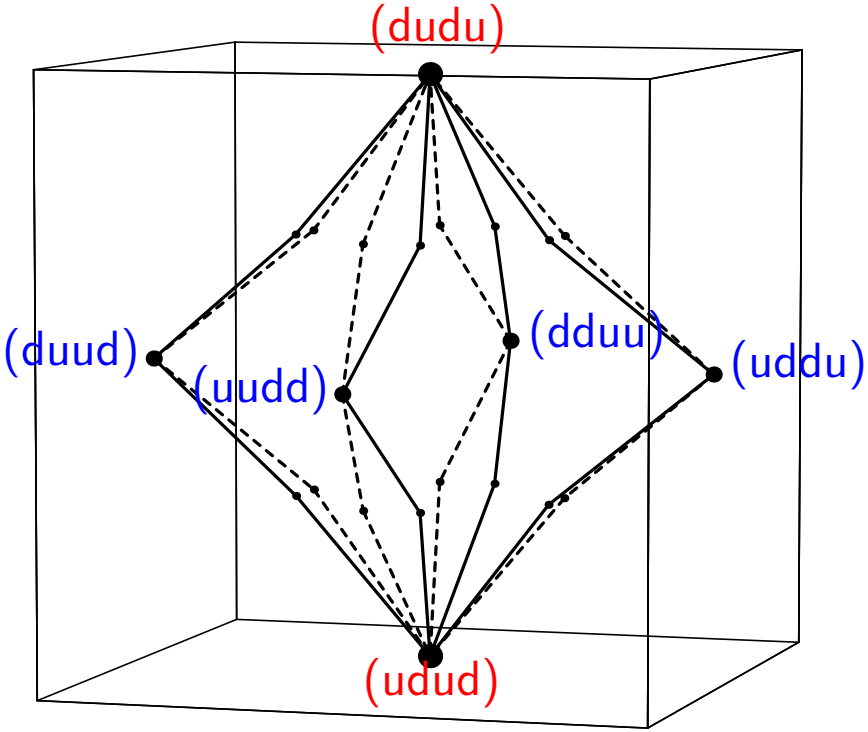

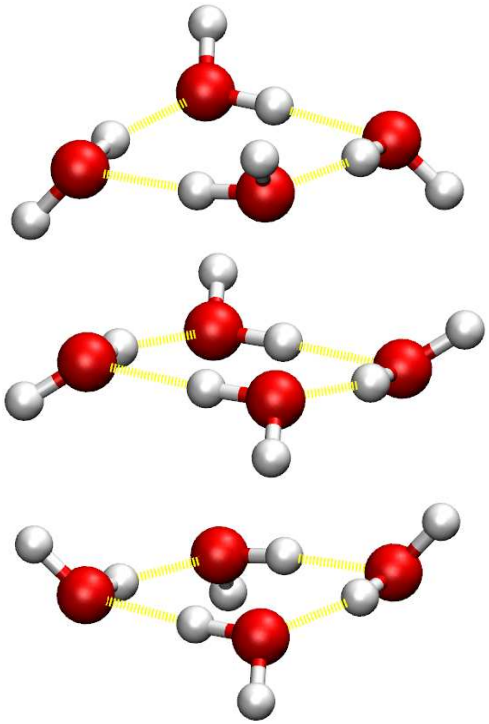

The global minimum of $(H_2O)_4$ is an S_4 unfrustrated ring; no low energy degenerate rearrangements have been found (one high energy bifurcation).

The experimental doublet splitting of 5.6 MHz for $(D_2O)_4$ is consistent with a quadruple flip, but is it concerted, sequential or delocalised over different structures? The direct bifurcation path gives a different splitting pattern.

Tunnelling in $(H_2O)_6$

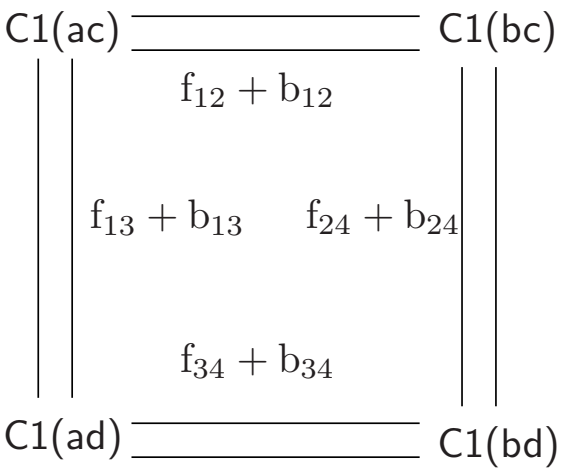

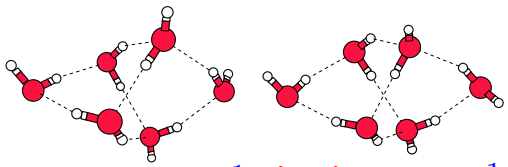

(C3) 27 cm^{-1} (C4) 57 cm^{-1}

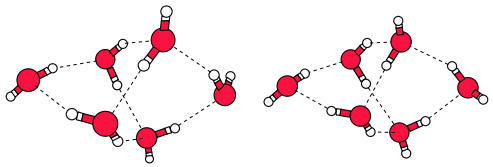

(C1) 0 cm^{-1} (C2) 13 cm^{-1}

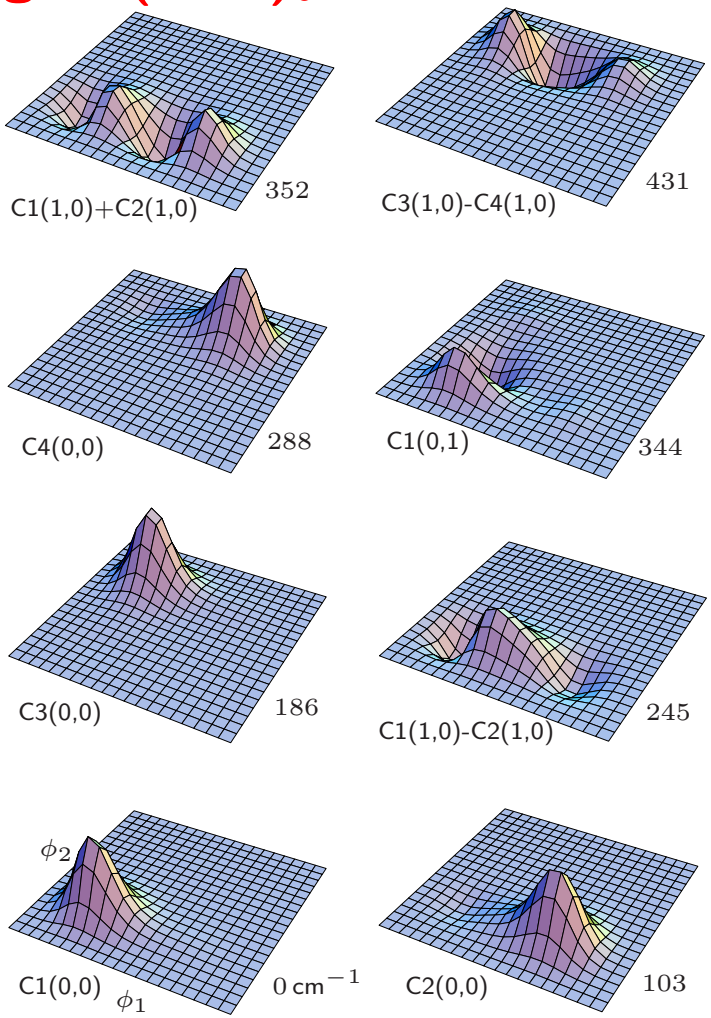

Four cage isomers interconvert through flip and bifurcation mechanisms. DVR calculations in the torsional space of 'dangling' hydrogens suggest delocalisation in excited states ('Theory of Atomic and Molecular Clusters', Springer, p. 86, 1999)

Path Integrals and Instanton Trajectories (*JCP*, **131**, 214106, 2009)

The ring polymer approximation to the quantum partition function $Q(T) = \mathrm{trace}\left[e^{-\beta\hat{H}}\right]$ is obtained by a Trotter factorisation into P imaginary time steps of length $\beta\hbar/P$. For particles of mass m and $\mathbf{x} = \{\mathbf{x}_1, \ldots, \mathbf{x}_P\}$:

$$Q(T) \approx \left(\frac{mP}{2\pi\beta\hbar^2}\right)^{P/2} \int e^{-\beta U_P(\mathbf{x})/P}\, d\mathbf{x},$$

$$\text{with} \qquad U_P(\mathbf{x}) = \sum_{\alpha=1}^{P} V(\mathbf{x}_\alpha) + \frac{mP^2}{2\beta^2\hbar^2} \sum_{\alpha=1}^{P} (\mathbf{x}_\alpha - \mathbf{x}_{\alpha+1})^2,$$

a mapping onto a classical ring polymer with P beads, each corresponding to a configuration of the physical system and coupled by harmonic springs.

Stationary points of $U_P(\mathbf{x})$ provide a finite-difference approximation to periodic instanton pathways, and hence rate constants. This approach also provides access to tunneling splittings for larger water clusters, where all degrees of freedom are treated quantum mechanically.

Disconnectivity Graphs

Disconnectivity graphs provide a powerful way to visualise the PES from a database of stationary points (Becker and Karplus).

At a given total energy, E, the minima can be grouped into disjoint sets, whose members are mutually accessible at that energy: each pair of minima in a set is connected directly or indirectly by a path with energy $< E$.

Connected graphs that contain no cycles are known as 'trees'.

'palm tree' 'weeping willow' 'banyan tree'

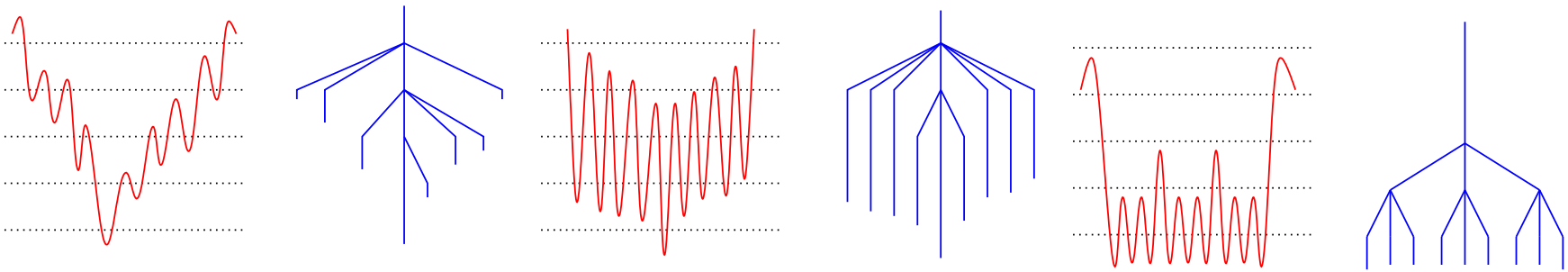

Catastrophe theory explains why short-range potentials result in surfaces that are globally flatter but locally rougher, while long-range potentials produce more pronounced potential energy funnels and efficient local relaxation.

Disconnectivity Graphs

Disconnectivity graphs provide a powerful way to visualise the PES from a database of stationary points (Becker and Karplus).

At a given total energy, E, the minima can be grouped into disjoint sets, whose members are mutually accessible at that energy: each pair of minima in a set is connected directly or indirectly by a path with energy $< E$.

Connected graphs that contain no cycles are known as 'trees'.

'palm tree' 'weeping willow' 'banyan tree'

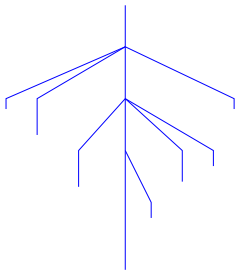

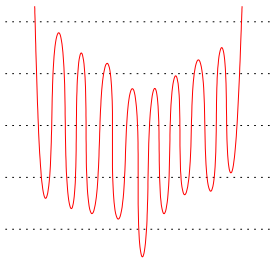

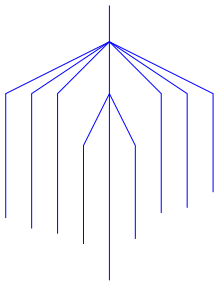

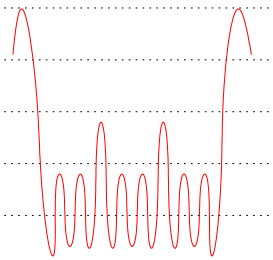

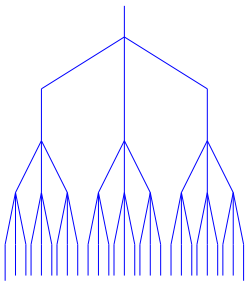

Catastrophe theory explains why short-range potentials result in surfaces that are globally flatter but locally rougher, while long-range potentials produce more pronounced potential energy funnels and efficient local relaxation.

Disconnectivity Graphs

Disconnectivity graphs provide a powerful way to visualise the PES from a database of stationary points (Becker and Karplus).

At a given total energy, E, the minima can be grouped into disjoint sets, whose members are mutually accessible at that energy: each pair of minima in a set is connected directly or indirectly by a path with energy $< E$.

Connected graphs that contain no cycles are known as 'trees'.

'palm tree' 'weeping willow' 'banyan tree'


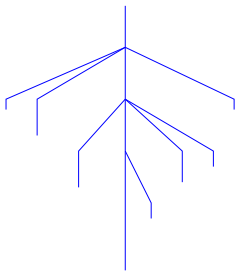
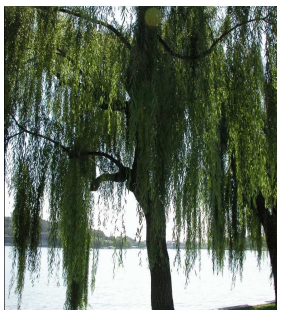
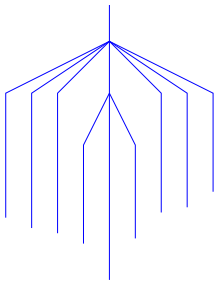
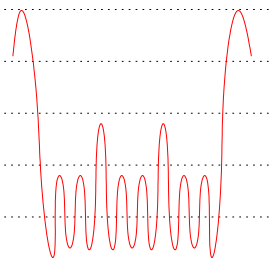
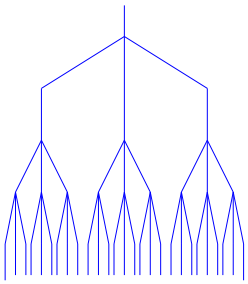

Catastrophe theory explains why short-range potentials result in surfaces that are globally flatter but locally rougher, while long-range potentials produce more pronounced potential energy funnels and efficient local relaxation.

Disconnectivity Graphs

Disconnectivity graphs provide a powerful way to visualise the PES from a database of stationary points (Becker and Karplus).

At a given total energy, E, the minima can be grouped into disjoint sets, whose members are mutually accessible at that energy: each pair of minima in a set is connected directly or indirectly by a path with energy $< E$.

Connected graphs that contain no cycles are known as 'trees'.

'palm tree' 'weeping willow' 'banyan tree'


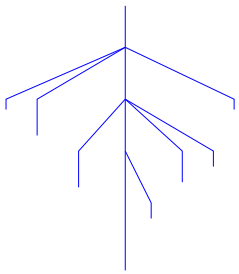
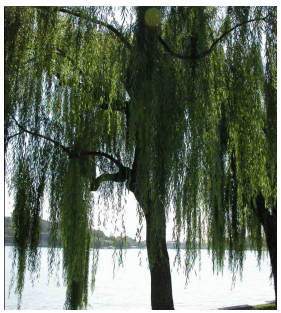
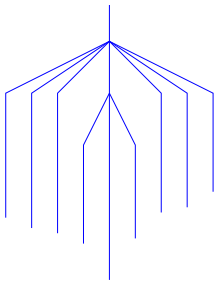

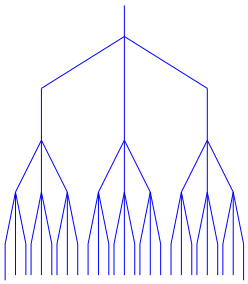

Catastrophe theory explains why short-range potentials result in surfaces that are globally flatter but locally rougher, while long-range potentials produce more pronounced potential energy funnels and efficient local relaxation.

Disconnectivity Graphs of 'Funnelled' Landscapes

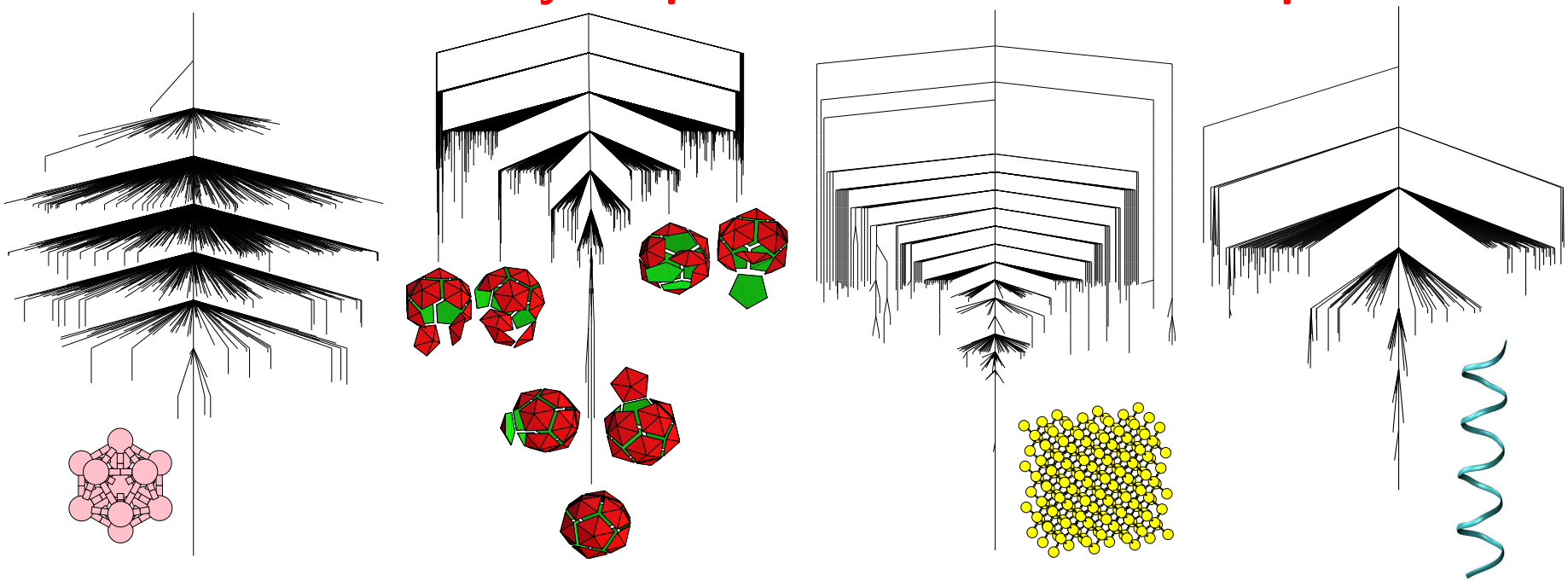

The nonrandom searches that result in magic number clusters, crystallisation, self-assembly, and protein folding are associated with a 'palm tree' organisation of the potential energy landscape (*Phil. Trans. Roy. Soc. A*, **363**, 357, 2005).

This 'funnelling' pattern has been verified for various structure-seeking systems, including the LJ_{13} cluster, icosahedral shells composed of pentagonal and hexagonal pyramids, crystalline (Stillinger-Weber) silicon, and the polyalanine ala_{16}. Large systems can exhibit relatively simple phenomenology.

Annealing of C_{60}

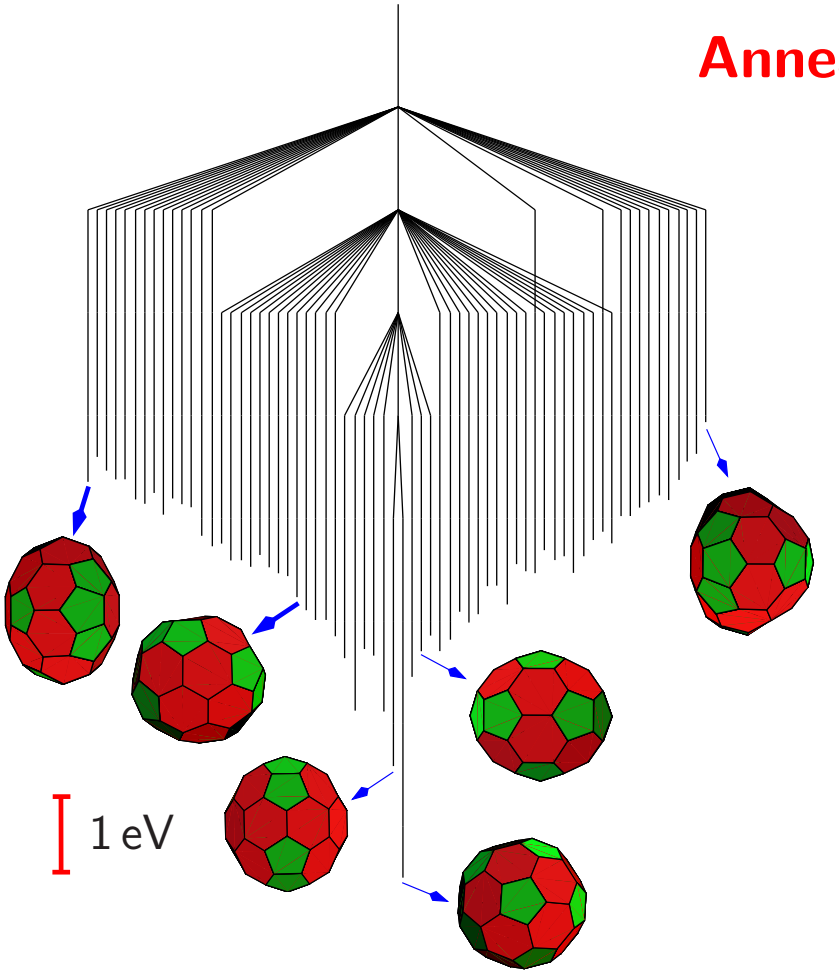

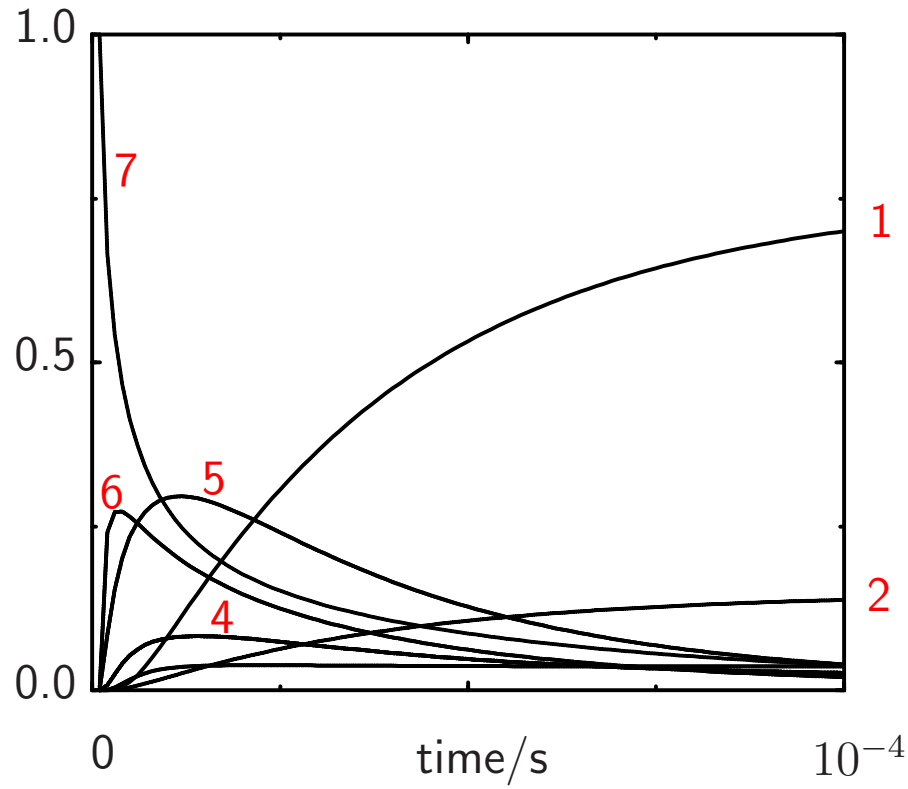

For C_{60} the long branches correspond to high barriers $\sim 4\,\mathrm{eV}$ (left). Relaxation from high energy fullerenes to the icosahedral global minimum occurs on a time scale of milliseconds if the temperature is high enough (right).

$(H_2O)_{20}$: A Nanodroplet

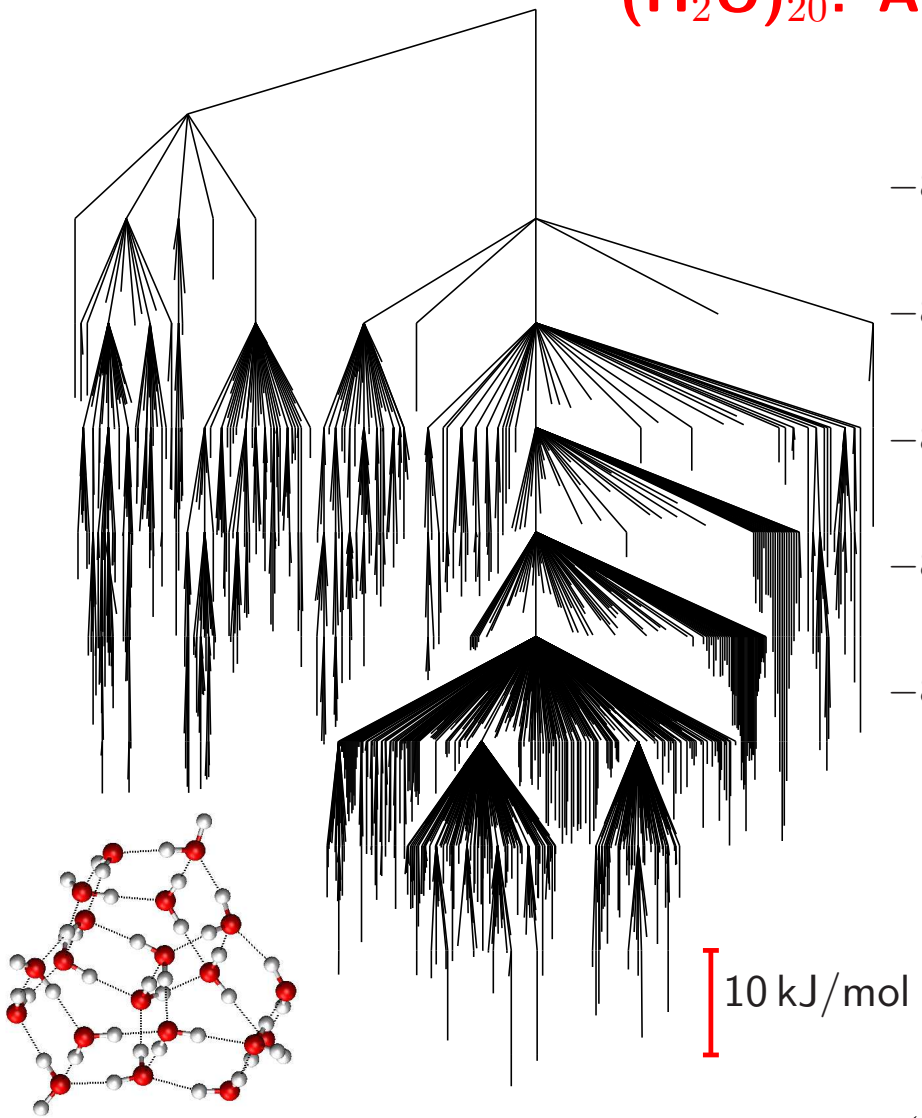

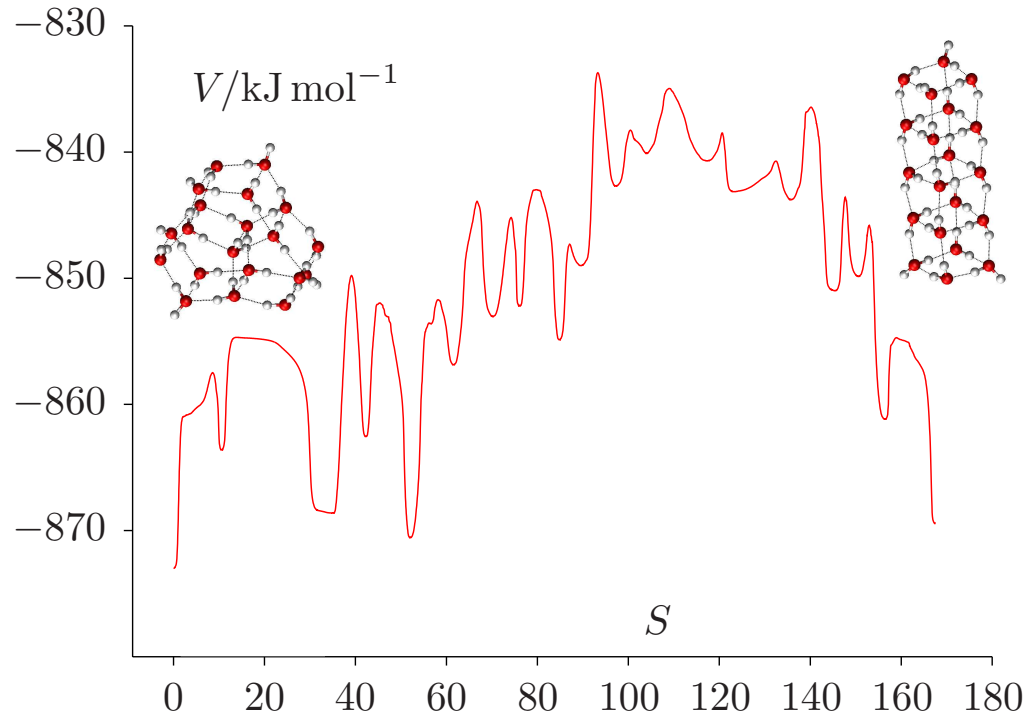

A disconnectivity graph for TIP4P $(H_2O)_{20}$ exhibits hierarchical structure: sets of minima are disconnected together. The interconversion rate between the pentagonal prism and box-kite morphologies at 40 K is around 10^{-37} s^{-1}.

Broken Ergodicity: LJ_{38} (*Phys. Rev. E*, **60**, 3701, 1999)

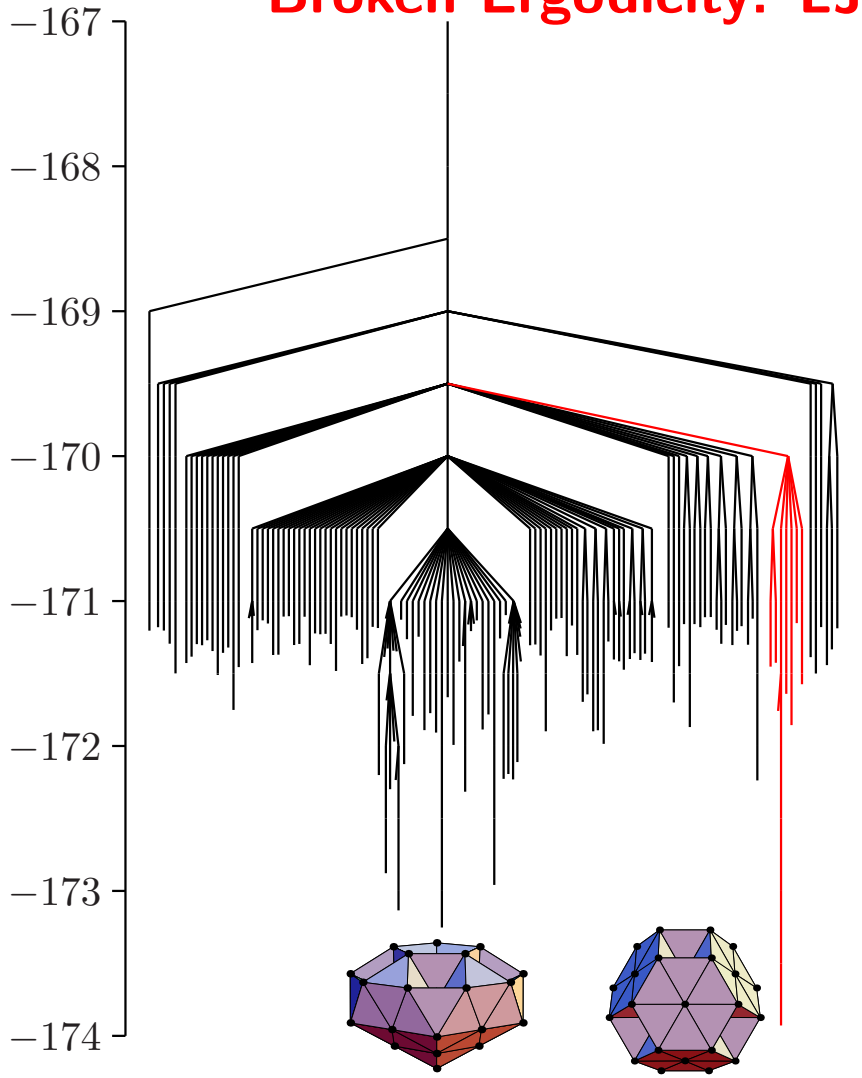

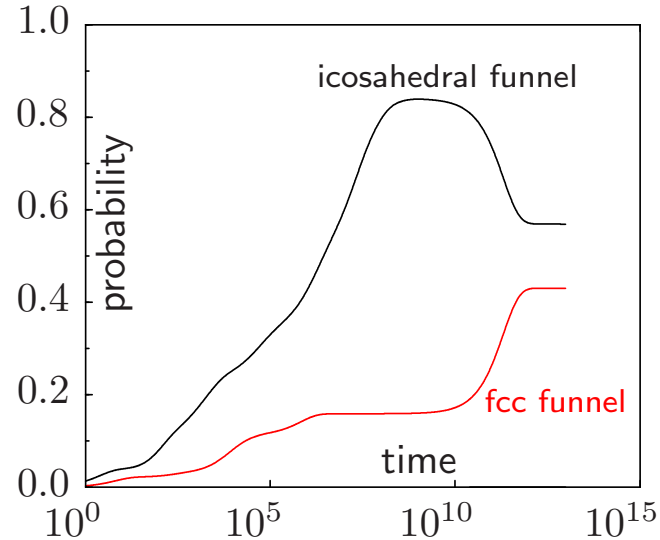

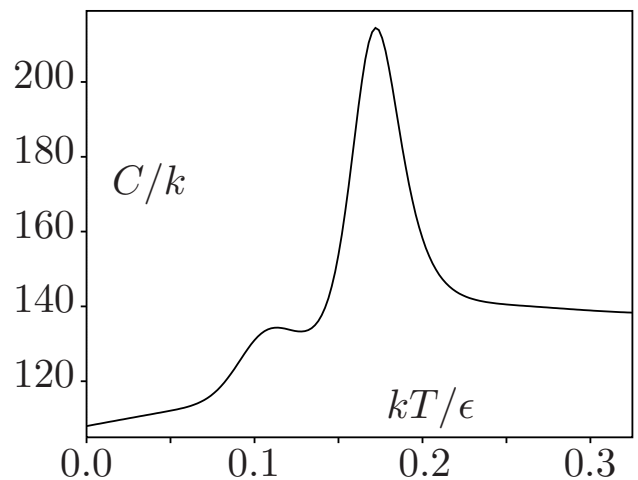

LJ_{38} exhibits a double funnel due to competition between icosahedral and truncated octahedral morphologies. The interconversion rate for Ar_{38} is calculated as $55\,s^{-1}$ at 14 K where a solid-solid transition occurs.

Glassy Landscapes (*J. Chem. Phys.*, **129**, 164507, 2008)

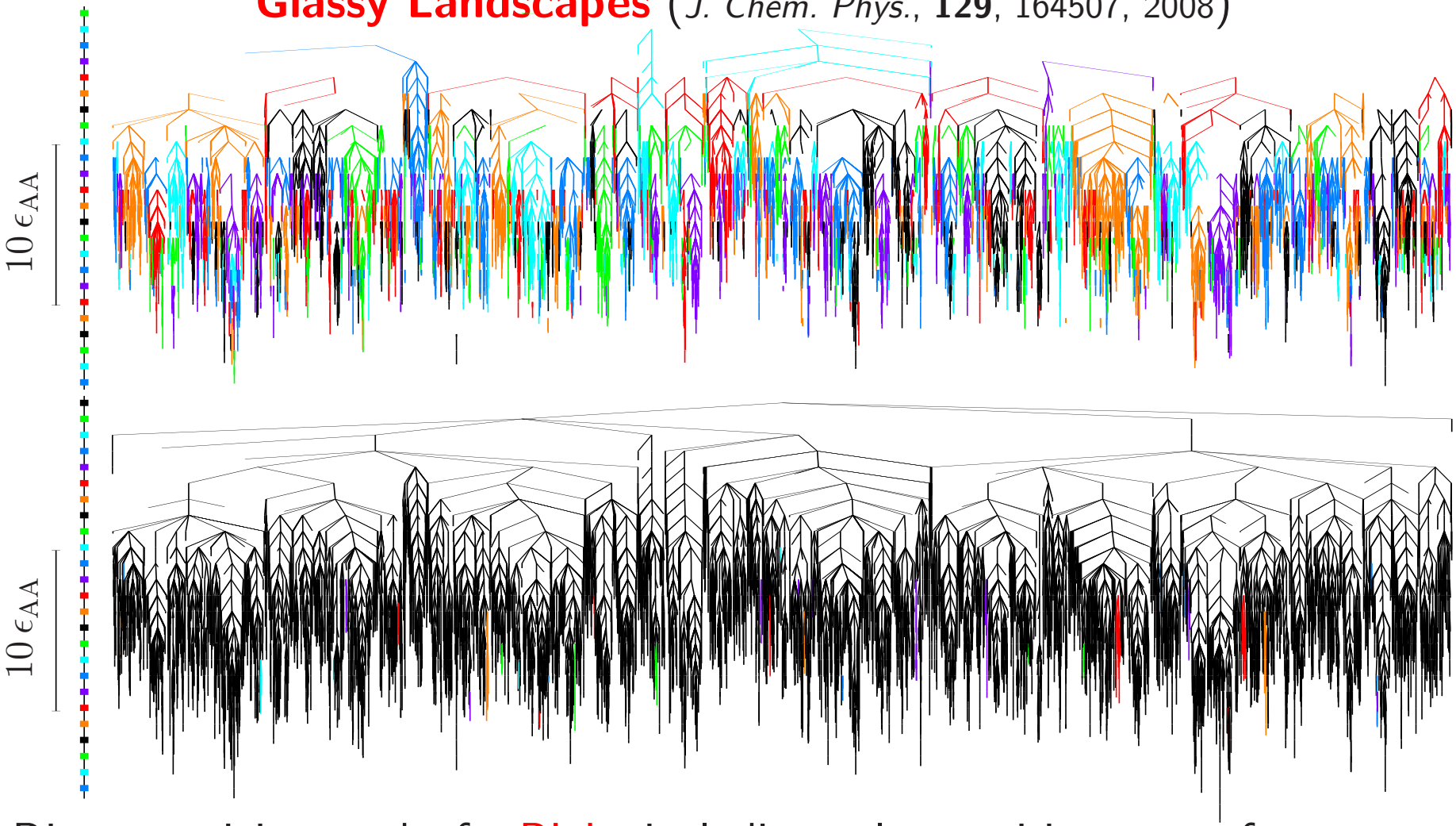

Disconnectivity graphs for BLJ_{60} including only transition states for noncage-breaking (top) and cage-breaking (bottom) paths. Changes in colour indicate disjoint sets of minima. Cage-breaking transitions, defined by two nearest-neighbour changes, define a higher order metabasin structure.

Basin-Hopping Global Optimisation

Transform the surface into basins of attraction: $\widetilde{E}(\mathbf{X}) = \min E(\mathbf{X})$.

Exploring $\tilde{E}(\mathbf{X})$ using Monte Carlo steps, following Li and Scheraga (*PNAS*, **84**, 6611, 1987), produced the lowest known minima for all LJ_n with $n \leq 110$ (*J. Phys. Chem. A*, **101**, 5111, 1997).

The transformation modifies both kinetics and thermodynamics.

Fortran code (`GMIN`) and database of structures: http://www-wales.ch.cam.ac.uk.

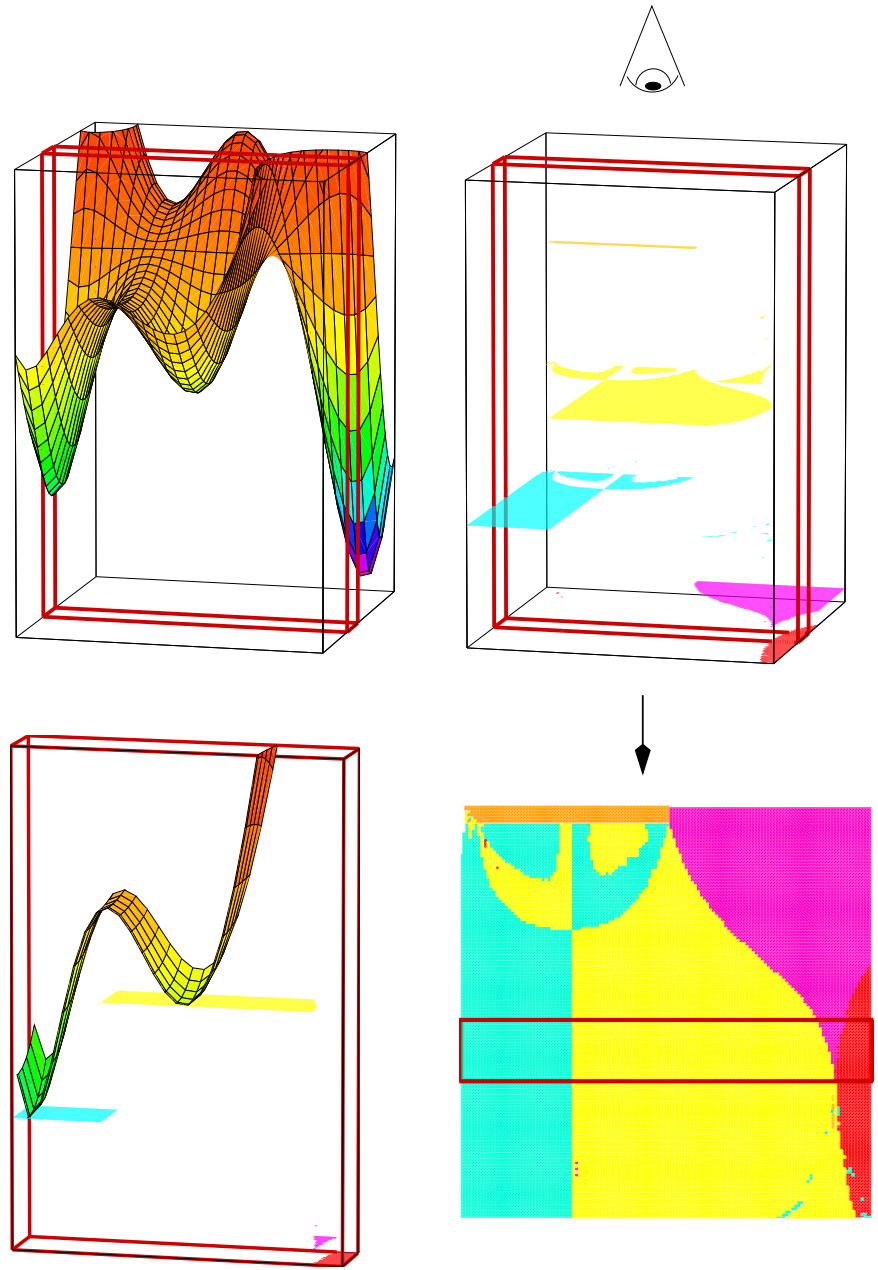

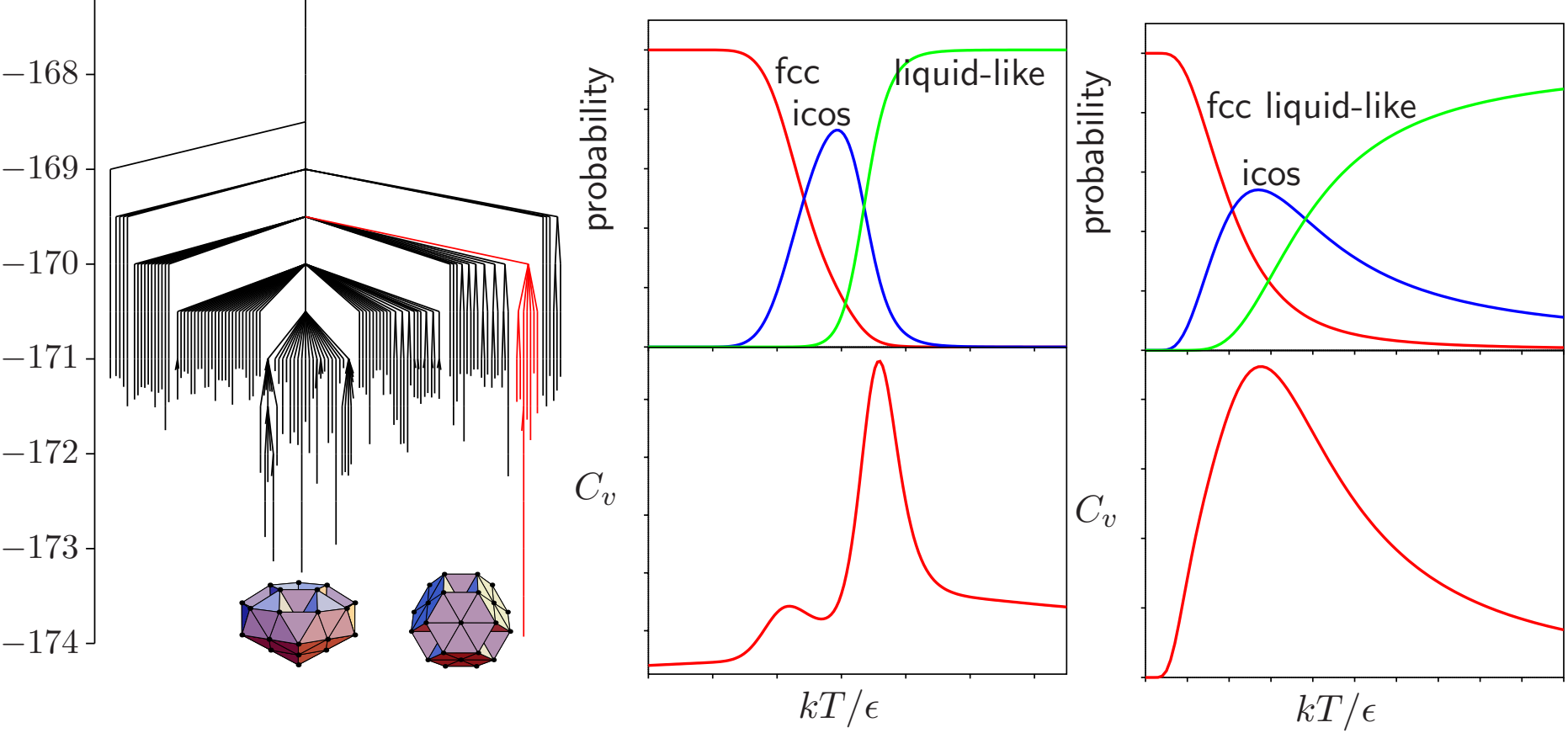

Basin-hopping succeeds for multi-funnel surfaces because the transitions are broadened (*Phys. Rev. Lett.*, **80**, 1357, 1998), giving a larger overlap in the probability distributions of different morphologies (right panels).

GMIN includes treatment of permutational isomerism, reseeding via taboo lists based on distance criteria, and exploitation of approximate symmetry.

Examples from the Cambridge Cluster Database Archives

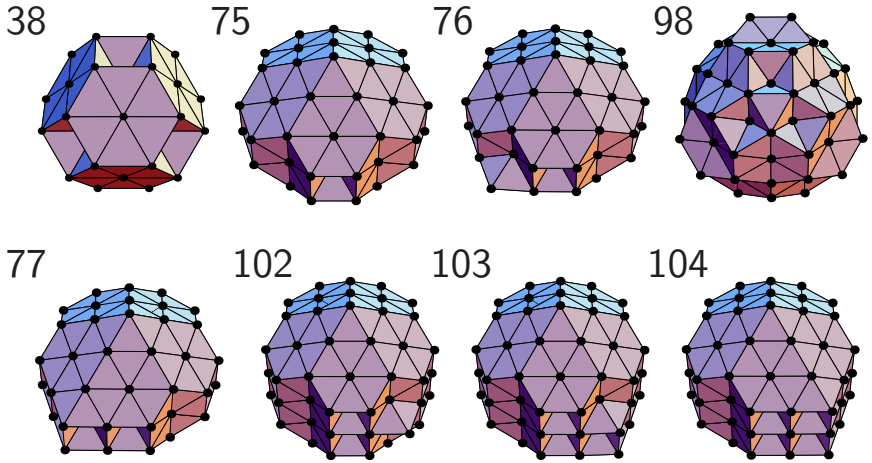

Non-icosahedral Lennard-Jones Clusters

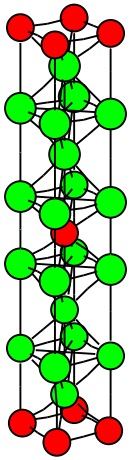

Binary LJ unit cell

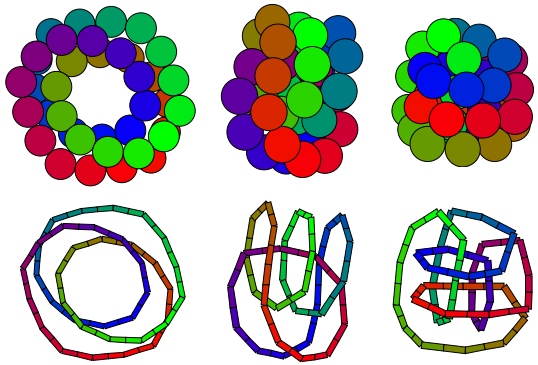

Stockmayer

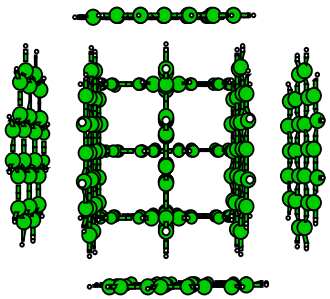

corronene$_{10}$

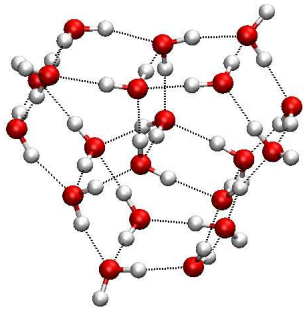

$(H_2O)_{20}$

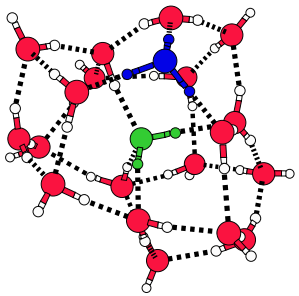

$H_3O^+(H_2O)_{20}$ Eigen

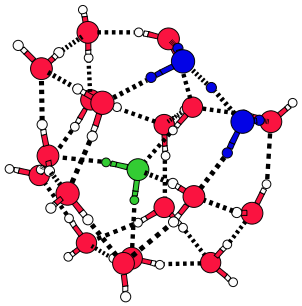

$H_3O^+(H_2O)_{20}$ Zundel

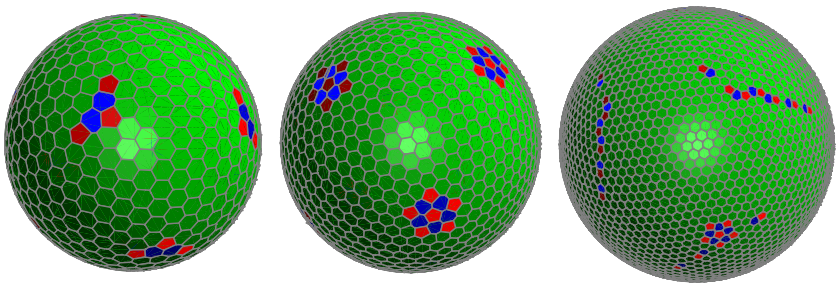

Thomson problem

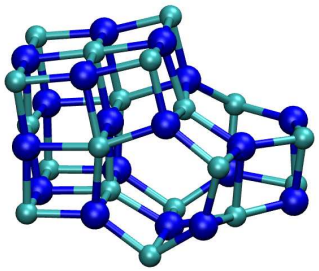

$(NaCl)_{18}Na^+$

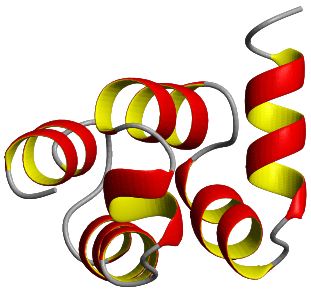

HYPA/FBP11

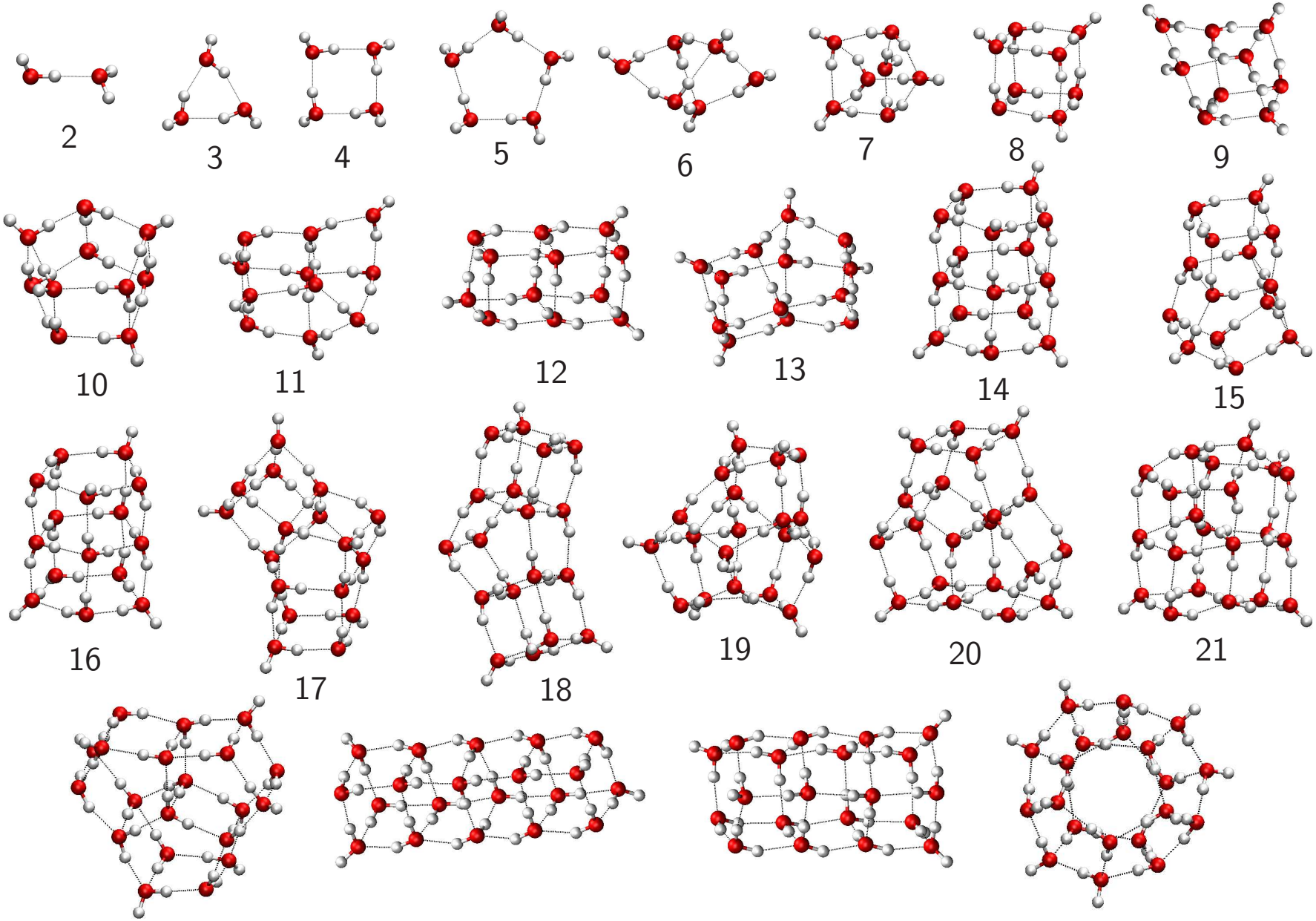

Global minima for TIP4P $(H_2O)_N$ and four morphologies of $(H_2O)_{20}$.

Transmembrane Oligomers of Aβ_{1-42} (*JACS*, **132**, 13300, 2010)

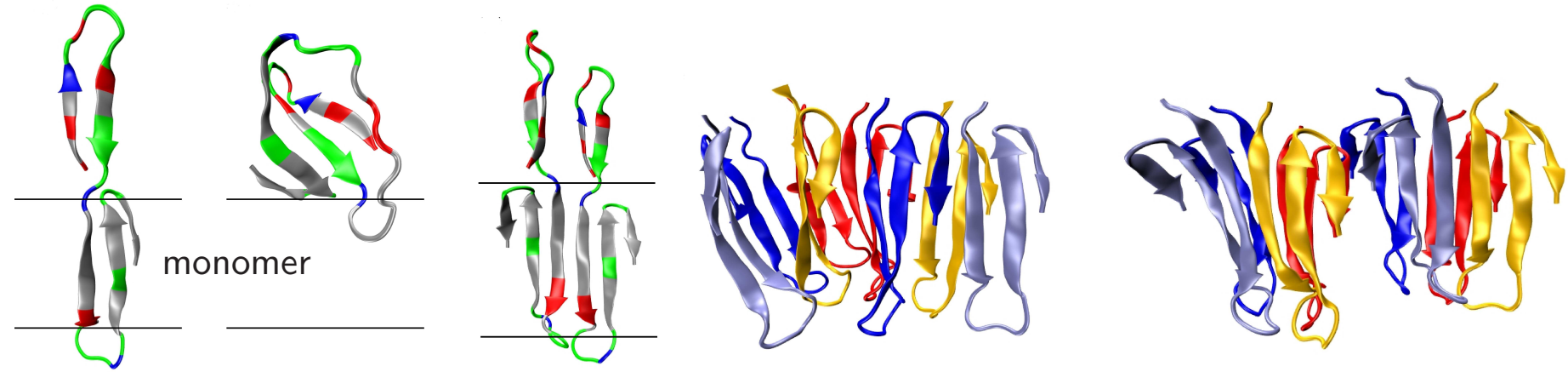

transmembrane surface dimer octamer structures: residues 17 to 42

Aβ_{1-42} oligomers up to the octamer have been investigated using CHARMM19 with the implicit membrane potential IMM1.

A basin-hopping/parallel tempering scheme with exchanges between basin-hopping runs at different temperatures was used, together with intra- and intermolecular coordinate moves for the peptides.

The most favourable monomer transmembrane structure has residues 17 to 42 inserted in the membrane. The most stable octamer structures can be viewed as displaced tetramers composed of two or three β-sheets.

An Extended Superposition Approach (*CPL*, **466**, 105, 2008)

The total partition function as a function of order parameter a is constructed as a superposition of contributions from local minima, $Z_i(a,T)$, and configurations taken from the pathways that connect them, $Z_r^\dagger(a,T)$:

$$Z_i(a,T) = \left(\frac{kT}{h\overline{\nu}_i}\right)^\kappa \frac{\exp\left(-V_i/kT\right)}{\sqrt{2\pi kTA_i}} \exp\left[-\frac{(a-a_i)^2}{2kTA_i}\right],$$

$$Z_r^\dagger(a,T) = \left(\frac{kT}{h}\right)^\kappa \frac{\delta_r \exp\left(-V_r^\dagger/kT\right)}{\left(\overline{\nu}_r^\dagger\right)^{\kappa-1} 2\pi kT\sqrt{A_r^\dagger}} \exp\left[-\frac{\left(a-a_r^\dagger\right)^2}{2kTA_r^\dagger}\right],$$

where $\overline{\nu}_i$ is the geometric mean of the normal mode frequencies, $\nu_{i,\gamma}$, V_i and a_i are the potential energy and order parameter for minimum i, $\kappa = 3N-6$, δ_r is a displacement, $\dagger$ labels transition states, and

$$A_i = \sum_{\gamma=1}^{\kappa} \left[\left.\frac{\partial a(\mathbf{q}_i)}{\partial q_{i,\gamma}}\right|_{\mathbf{q}_i=\mathbf{0}} \frac{1}{2\pi\nu_{i,\gamma}}\right]^2.$$

The method can be extended for projections onto additional order parameters.

Free energy surfaces for alanine dipeptide (CHARMM22/vacuum) from superposition, replica exchange, and reaction path Hamiltonian superposition:

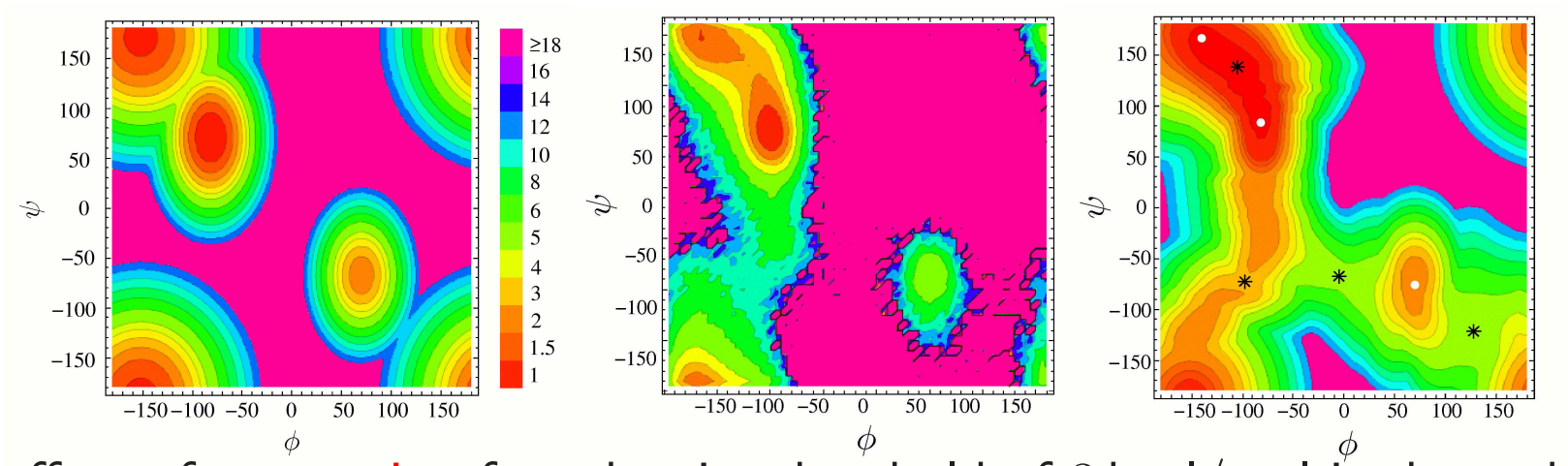

The effect of regrouping for a barrier threshold of $3\,\mathrm{kcal/mol}$ is shown below for AMBER(ff03)/GB^{OCB}; this approach avoids the 'filling in' problem.

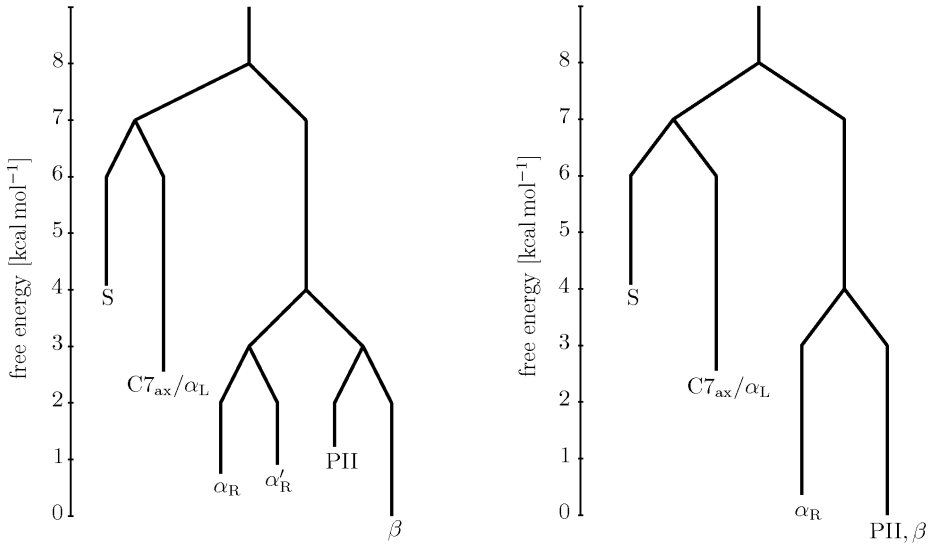

Thermodynamics for Ala_4 in Vacuum: CHARMM

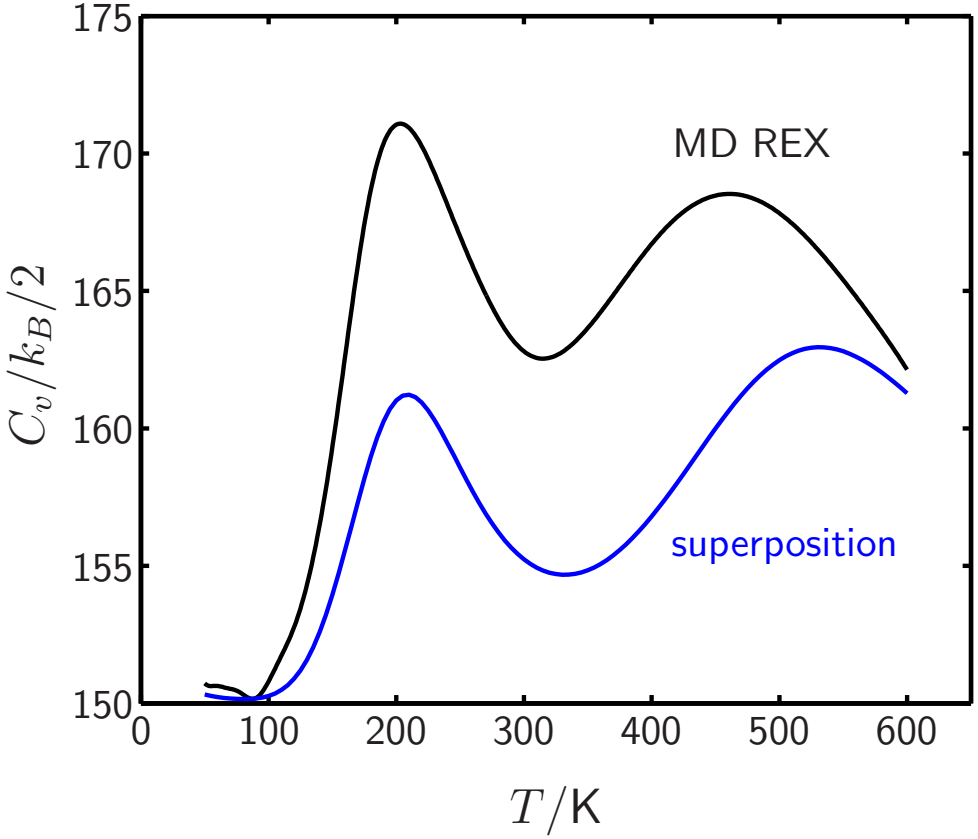

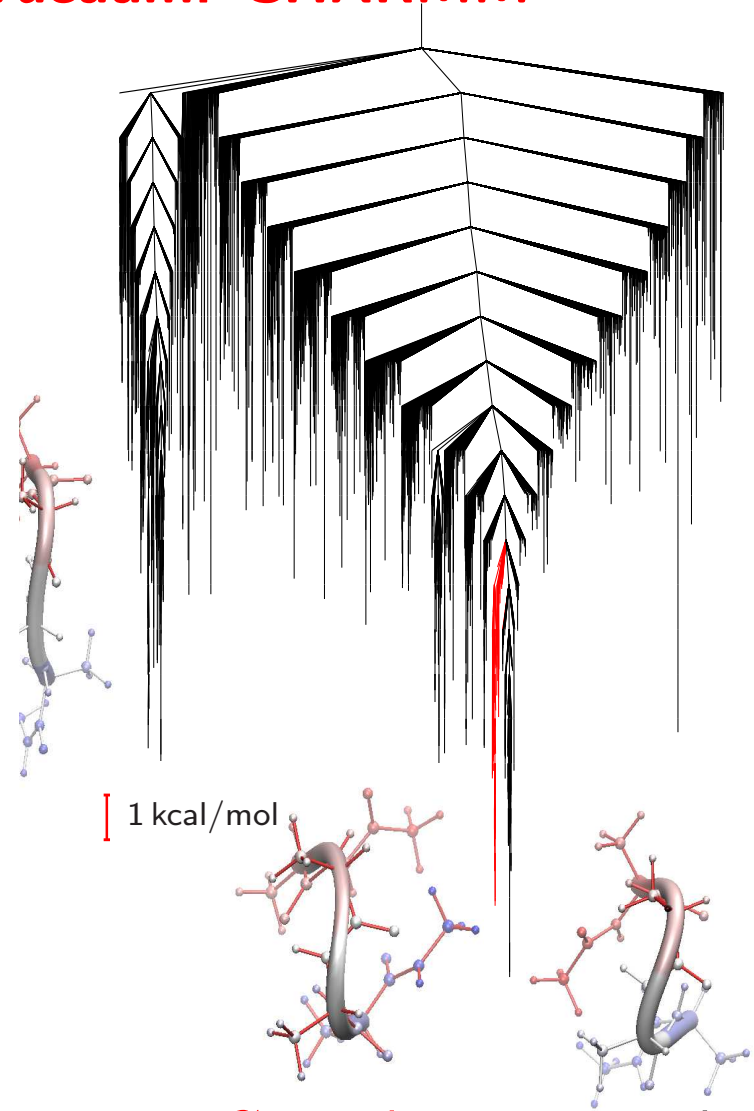

Ala_4 in vacuum (charmm27) has a low temperature C_v peak, corresponding to the hundred or so lowest minima in the disconnectivity graph. The high temperature peak corresponds to the finite system analogue of melting.

Thermodynamics for Ala_4 in Vacuum: AMBER

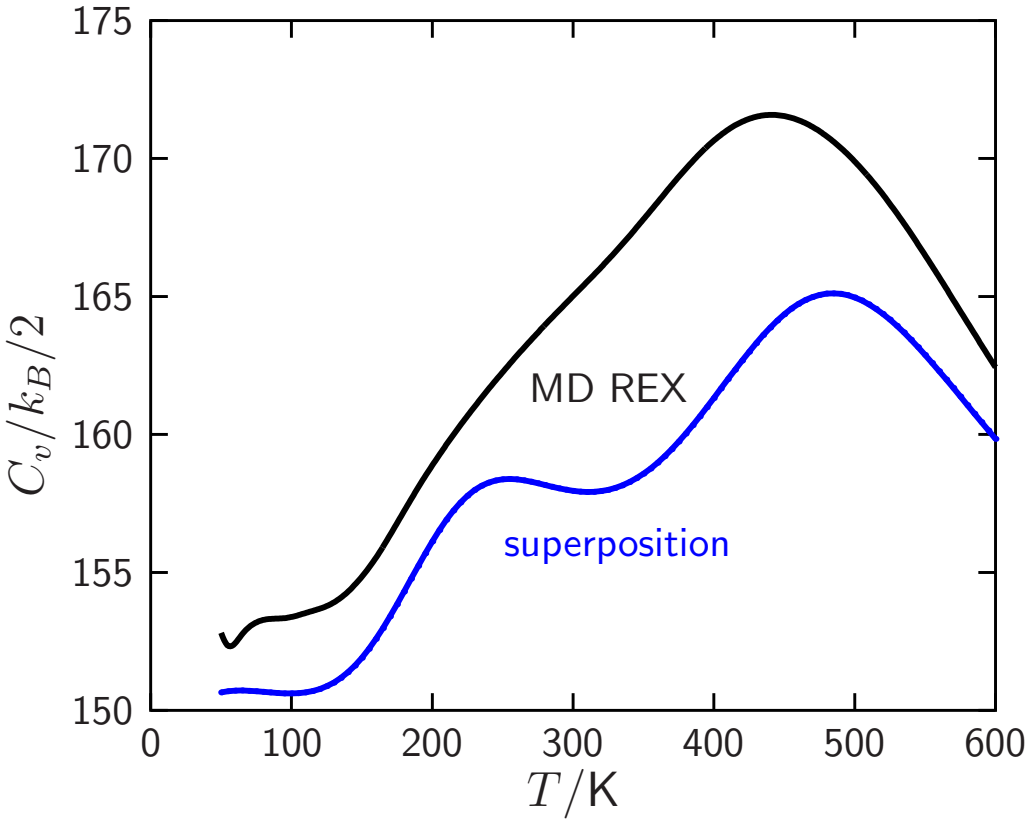

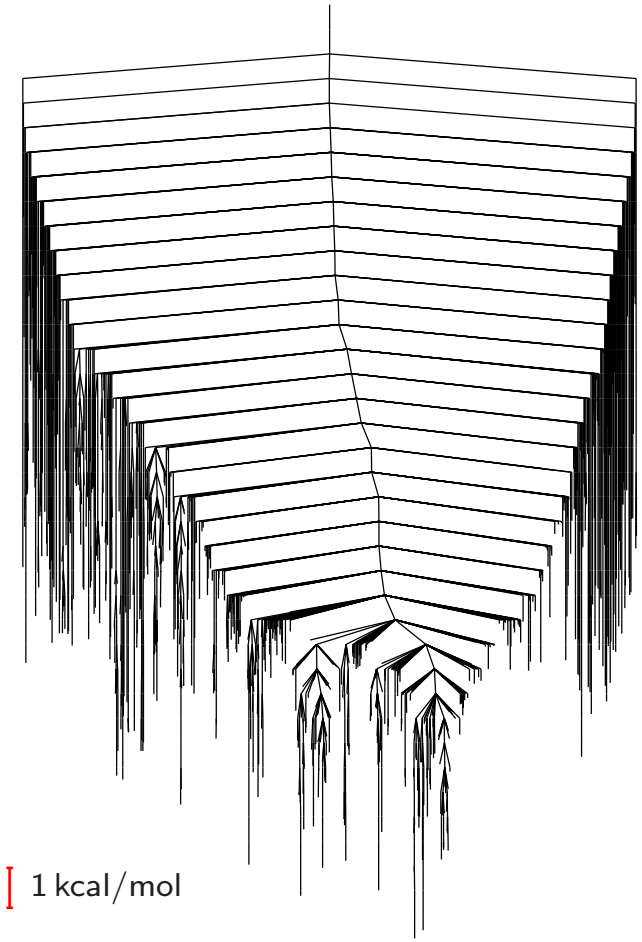

Ala_4 in vacuum (amber99sb) appears to be similar to CHARMM.

Thermodynamics for Ala_4 in Vacuum: AMBER

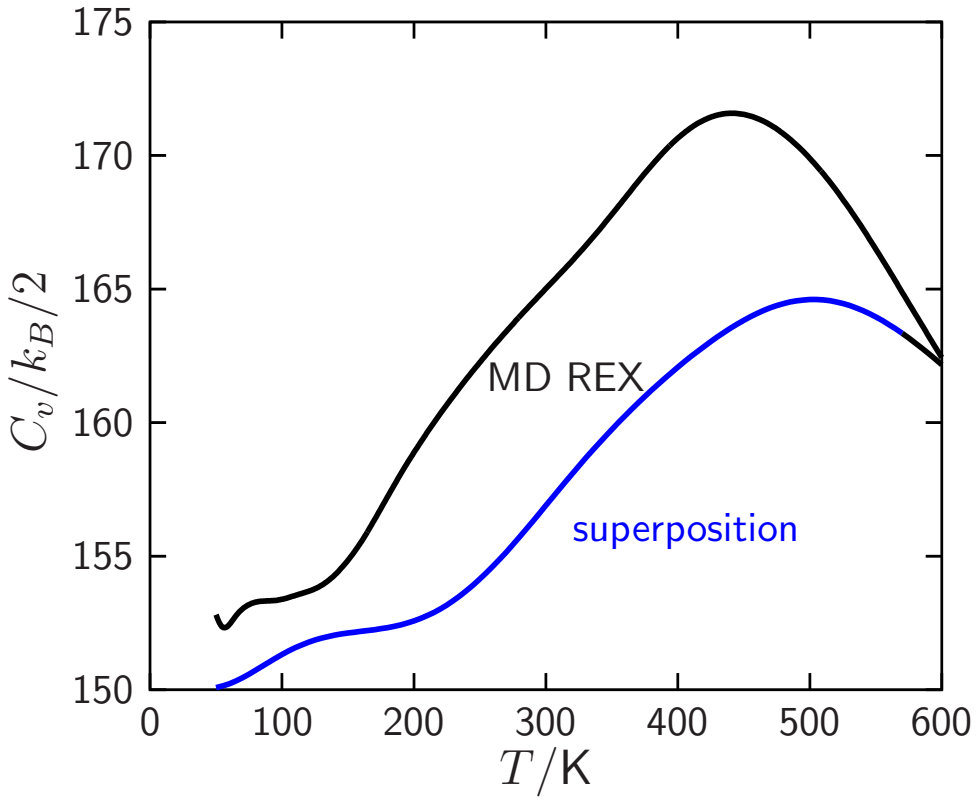

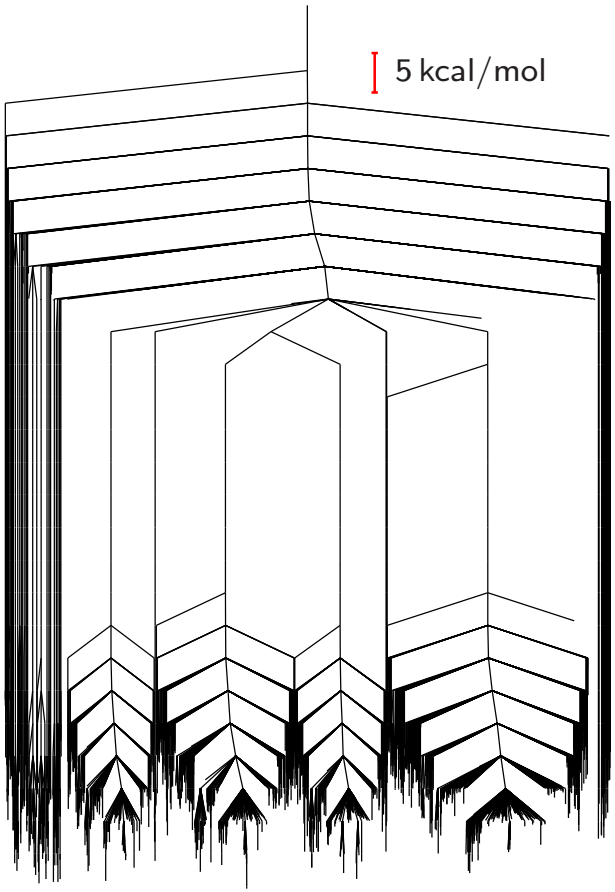

In fact, the global minimum for this potential has a mixture of L and D amino acids. The landscape separates into regions with different L/D composition, spearated by barriers of order 90 kcal/mol.

Discrete Path Sampling (*Mol. Phys.*, **100**, 3285, 2002; **102**, 891, 2004).

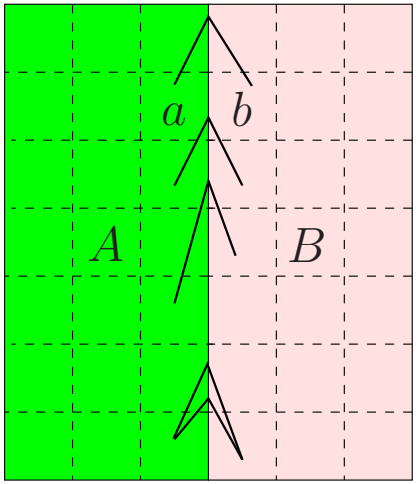

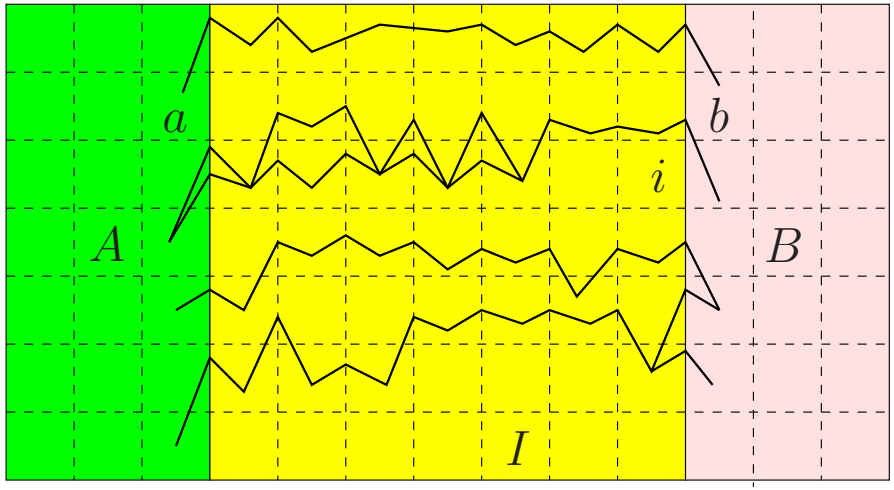

no intervening minima

$$\frac{p_a(t)}{p_{a'}(t)} = \frac{p_a^{\rm eq}}{p_{a'}^{\rm eq}} \qquad \dot{p}_i(t) = 0 \qquad \frac{p_b(t)}{p_{b'}(t)} = \frac{p_b^{\rm eq}}{p_{b'}^{\rm eq}}$$

Phenomenological $A \leftrightarrow B$ rate constants can be formulated as sums over discrete paths, defined as sequences of local minima and the transition states that link them, weighted by equilibrium occupation probabilities, $p_b^{\rm eq}$:

$$k_{AB}^{\rm SS} = \frac{1}{p_B^{\rm eq}} \sum_{a \leftarrow b} P_{a i_1} P_{i_1 i_2} \cdots P_{i_{n-1} i_n} P_{i_n b} \tau_b^{-1} p_b^{\rm eq} = \frac{1}{p_B^{\rm eq}} \sum_{b \in B} \frac{C_b^A p_b^{\rm eq}}{\tau_b},$$

where $P_{\alpha\beta}$ is a branching probability and C_b^A is the committor probability that the system will visit an A minimum before it returns to the B region.

Discrete path sampling builds connected databases of stationary points that are relevant to global kinetics (*Int. Rev. Phys. Chem.*, **25**, 237, 2006).

The paths that make the largest contributions to k_{AB}^{SS} can be extracted using the Dijkstra or recursive enumeration algorithms, using edge weights $-\ln P_{\alpha\beta}$ (*J. Chem. Phys.*, **121**, 1080, 2004; *J. Phys. Chem. B*, **112**, 8760, 2008).

A hierarchy of expressions can be obtained for the rate constants:

$$k_{AB}^{\mathrm{SS}} = \frac{1}{p_B^{\mathrm{eq}}} \sum_{b \in B} \frac{C_b^A p_b^{\mathrm{eq}}}{\tau_b}, \quad k_{AB}^{\mathrm{NSS}} = \frac{1}{p_B^{\mathrm{eq}}} \sum_{b \in B} \frac{C_b^A p_b^{\mathrm{eq}}}{t_b}, \quad k_{AB} = \frac{1}{p_B^{\mathrm{eq}}} \sum_{b \in B} \frac{p_b^{\mathrm{eq}}}{\mathcal{T}_{Ab}}.$$

τ_b, t_b and $\mathcal{T}_{Ab}$ are the mean waiting times for a transition from b to an adjacent minimum, to any member of $A \cup B$, and to the A set, with $\tau_b \leq t_b \leq \mathcal{T}_{Ab}$.

k_{AB} is formally exact within a Markov assumption for transitions between the states, which can be regrouped. Additional approximations come from incomplete sampling, and the densities of states and the unimolecular rate theory used to describe the local thermodynamics and kinetics.

Discrete Path Sampling Examples I

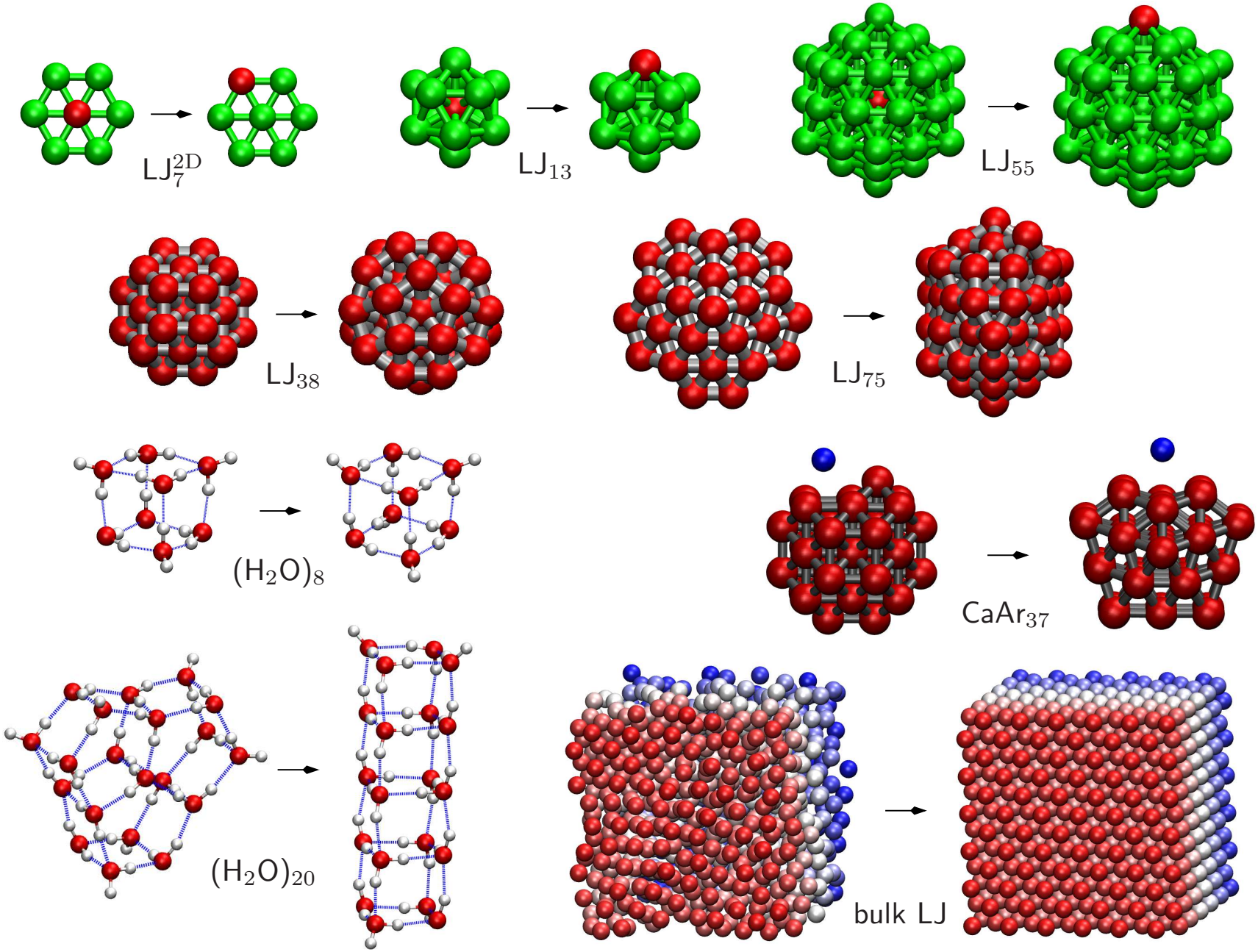

Discrete Path Sampling Examples II

Ala_{16} ↓

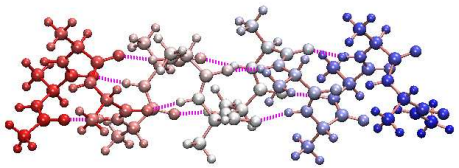

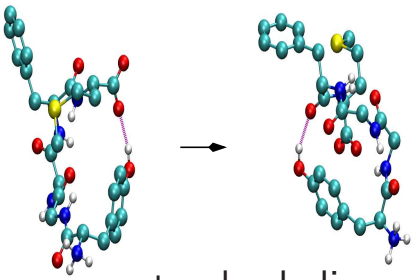

met-enkephalin

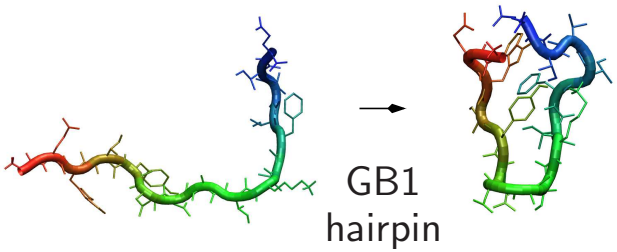

GB1 hairpin

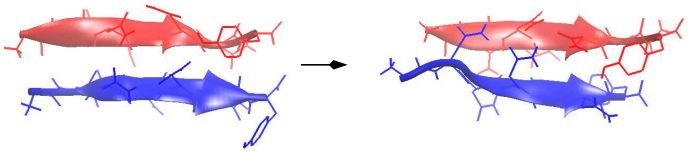

GNNQQNY

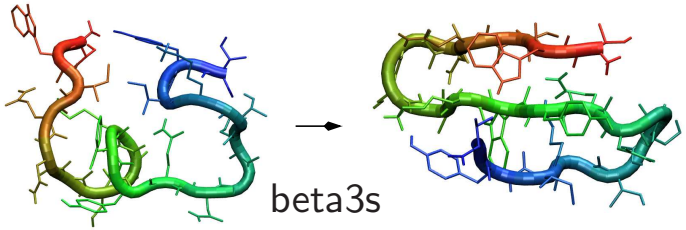

beta3s

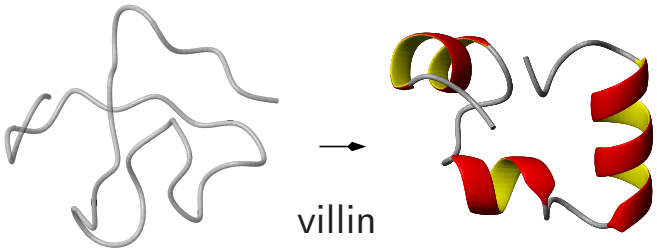

villin

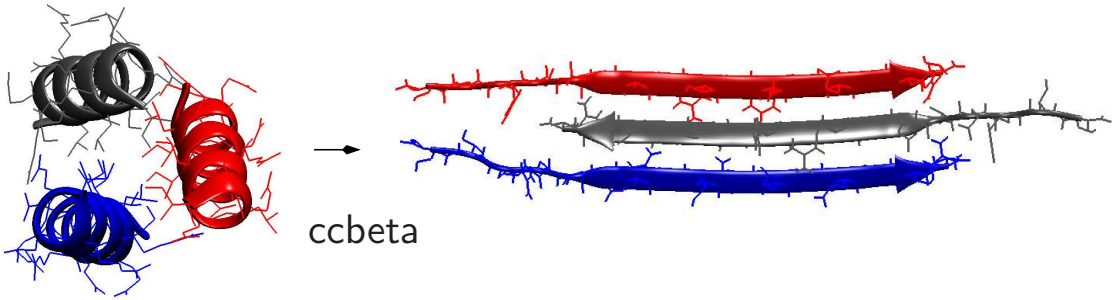

ccbeta

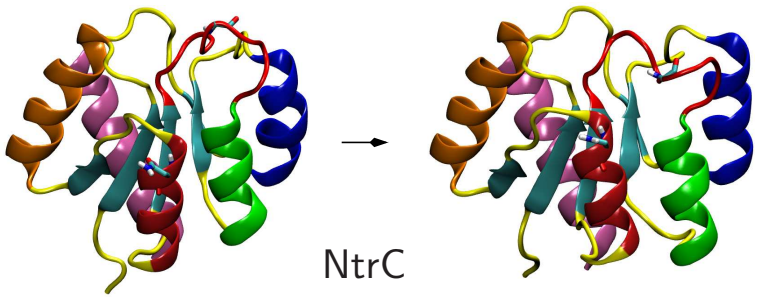

NtrC

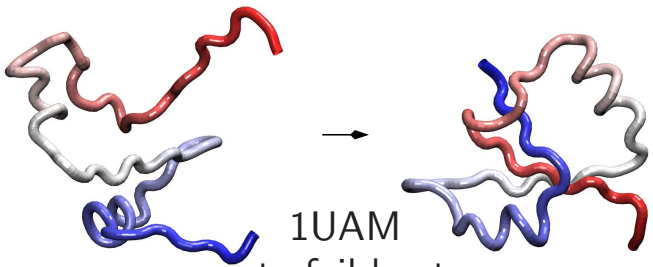

1UAM trefoil knot

THE JOURNAL OF CHEMICAL PHYSICS **135**, 034108 (2011)

Simulating structural transitions by direct transition current sampling: The example of LJ_{38}

Massimiliano Picciani,[1,a)] Manuel Athènes,[1] Jorge Kurchan,[2] and Julien Tailleur[3]
[1]*CEA, DEN, Service de Recherches de Métallurgie Physique, F-91191 Gif-sur-Yvette, France*
[2]*CNRS; ESPCI, 10 rue Vauquelin, UMR 7636 PMMH, 75005 Paris, France*
[3]*School of Physics of Astronomy, SUPA, University of Edinburgh, The King's Buildings, Mayfield Road, EH9 3JZ Edinburgh, United Kingdom*

(Received 2 March 2011; accepted 21 June 2011; published online 20 July 2011)

Another attempt to study the transitions between the two funnels of LJ_{38} relies on the use of transition path sampling.[33] Because of the number of metastable states separating the two main basins, the traditional shooting and shifting algorithm failed here, despite previous success for smaller LJ clusters.[39] The authors thus developed a two-ended approach which manages to successfully locate reaction paths between the two basins: they started from a straight trial trajectory linking the two minima, and obtained convergence towards trajectories of energies similar to those obtained in the discrete path sampling approach.[33] Although the authors point out the lack of ergodicity in the sampling within their approach and the sensitivity on the "discretization" of the trajectories, this is nevertheless a progress and the main drawback remains the high computational cost (the work needed 10^5 h of central processing unit (cpu) time) to obtain such converged trajectories. In contrast, the simulations we present below required less than 10^2 h of cpu time.

Geometry Optimisation

Minimisation: Nocedal's algorithm, LBFGS, with line searches removed.

Transition states: single-ended searches use hybrid eigenvector-following ('Defect Migration in Crystalline Silicon', *Phys. Rev. B*, **59**, 3969, 1999); double-ended searches use the doubly-nudged elastic band approach (*J. Chem. Phys.*, **120**, 2082, 2004; *cf.* Henkelman and Jónsson).

The `GMIN` (global optimisation), `OPTIM` (transition states and pathways) and `PATHSAMPLE` (discrete path sampling) programs are available under the Gnu General Public License. Access to the svn source can be arranged for developers. Current svn tarball image: http://www-wales.ch.cam.ac.uk.

Interfaces to many electronic structure codes are included. Example: split interstitial migration in crystalline silicon (*Chem. Phys. Lett.*, **341**, 185, 2001).

A Knotted Protein (*PLoS Comput. Biol.*, **6**, e1000835, 2010)

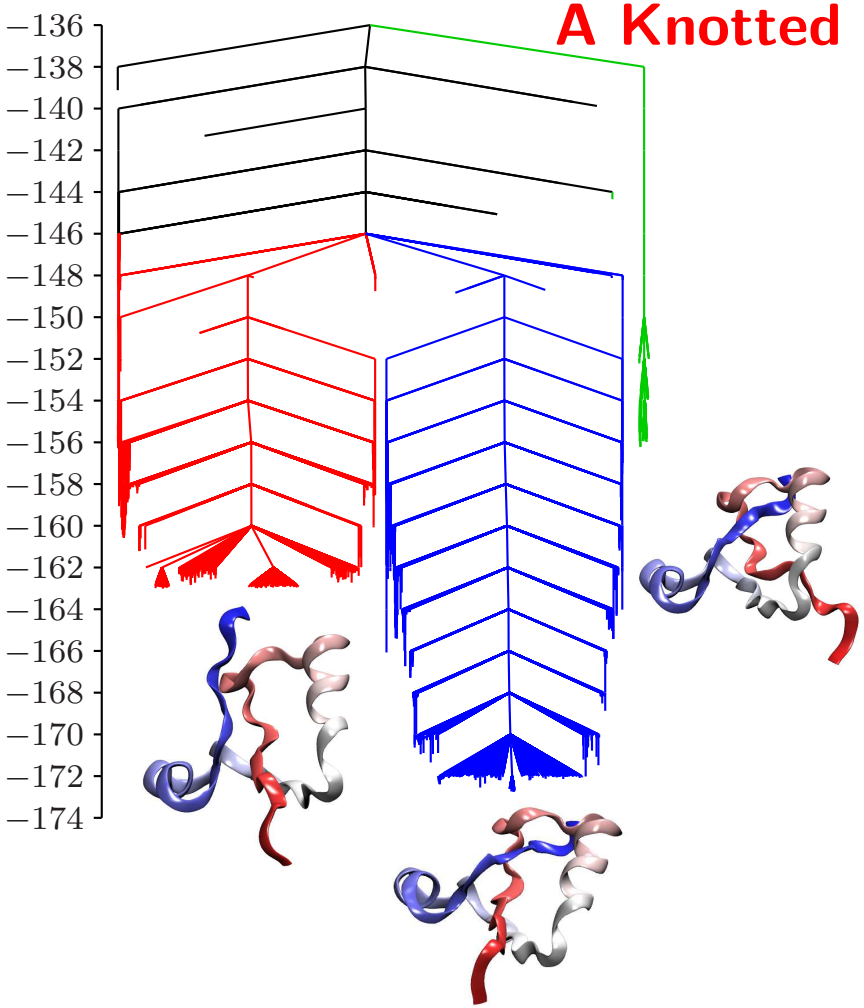

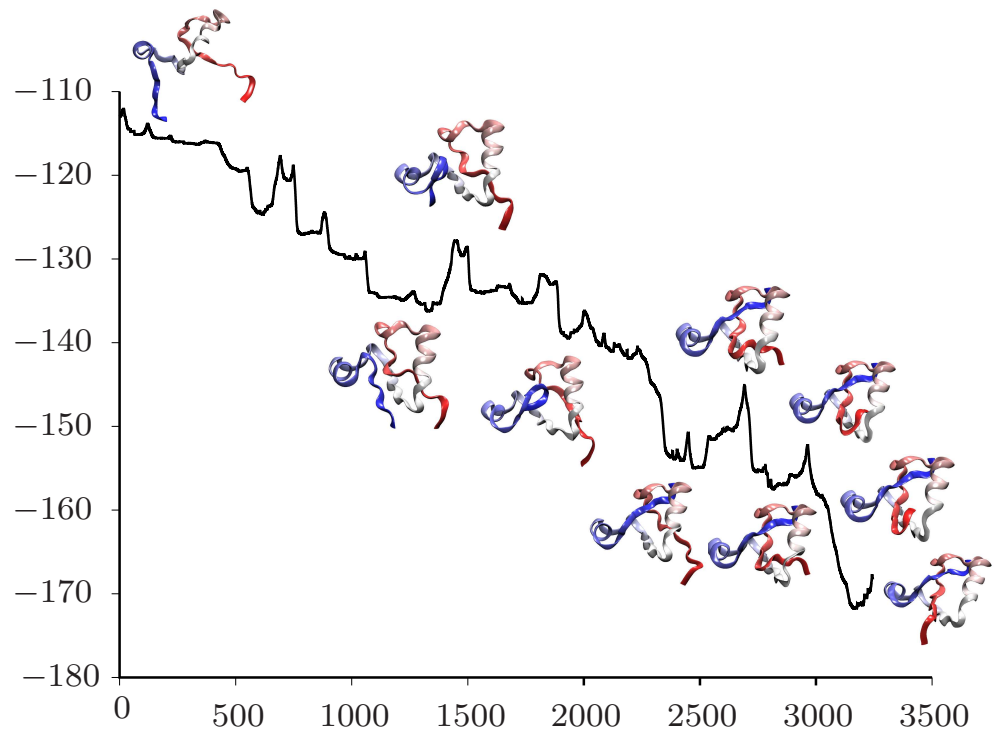

The tRNA methyltransferase protein 1UAM contains a deep trefoil knot.

The folding pathway has two slipknot-type steps for a truncated (residues 78–135) Gō model representation using an associated memory Hamiltonian.

The estimated rate constant is between 0.04 and 0.4 s^{-1}.

Angle-Axis Coordinates for Rigid Bodies (*PCCP*, **11**, 1970, 2009)

Rodrigues' formula for the rotation matrix **R** corresponding to a rotation of magnitude $\theta = (p_1^2 + p_2^2 + p_3^2)^{1/2}$ around the axis defined by $\mathbf{p}$ is

$$\mathbf{R} = \mathbf{I} + (1 - \cos\theta)\widetilde{\mathbf{p}}\widetilde{\mathbf{p}} + \sin\theta\,\widetilde{\mathbf{p}},$$

where $\mathbf{I}$ is the identity matrix, and $\widetilde{\mathbf{p}}$ is the skew-symmetric matrix

$$\widetilde{\mathbf{p}} = \frac{1}{\theta}\begin{pmatrix} 0 & -p_3 & p_2 \\ p_3 & 0 & -p_1 \\ -p_2 & p_1 & 0 \end{pmatrix}.$$

The product of $\widetilde{\mathbf{p}}$ and any vector $\mathbf{v}$ returns the cross product: $\widetilde{\mathbf{p}}\mathbf{v} = \hat{\mathbf{p}} \times \mathbf{v}$.

All terms involving rigid-body angle-axis coordinates can be obtained by the action of the rotation matrix and its derivatives, whose forms are programmed in system-independent subroutines.

The angle-axis representation is free of singularities and constraints.

1st derivatives: $\mathbf{R}_k \equiv \dfrac{\partial \mathbf{R}}{\partial p_k} = \dfrac{p_k \sin\theta}{\theta}\,\widetilde{\mathbf{p}}^2 + (1-\cos\theta)(\widetilde{\mathbf{p}}_k\widetilde{\mathbf{p}} + \widetilde{\mathbf{p}}\widetilde{\mathbf{p}}_k) + \dfrac{p_k\cos\theta}{\theta}\widetilde{\mathbf{p}} + \sin\theta\,\widetilde{\mathbf{p}}_k$, with $\widetilde{\mathbf{p}}_1 = \dfrac{1}{\theta^3}\begin{pmatrix} 0 & p_1p_3 & -p_1p_2 \\ -p_1p_3 & 0 & p_1^2-\theta^2 \\ p_1p_2 & \theta^2-p_1^2 & 0 \end{pmatrix}$

2nd derivatives : $\mathbf{R}_{kk} \equiv \dfrac{\partial^2 \mathbf{R}}{\partial p_k^2} = \dfrac{2p_k\sin\theta}{\theta}(\widetilde{\mathbf{p}}_k\widetilde{\mathbf{p}} + \widetilde{\mathbf{p}}\widetilde{\mathbf{p}}_k) + \left(\dfrac{p_k^2\cos\theta}{\theta^2} - \dfrac{p_k^2\sin\theta}{\theta^3} + \dfrac{\sin\theta}{\theta}\right)\widetilde{\mathbf{p}}^2$

$$+\ (1-\cos\theta)(2\widetilde{\mathbf{p}}_k^2 + \widetilde{\mathbf{p}}_{kk}\widetilde{\mathbf{p}} + \widetilde{\mathbf{p}}\widetilde{\mathbf{p}}_{kk}) + (-\frac{p_k^2\sin\theta}{\theta^2} - \frac{p_k^2\cos\theta}{\theta^3} + \frac{\cos\theta}{\theta})\widetilde{\mathbf{p}} + \frac{2p_k\cos\theta}{\theta}\widetilde{\mathbf{p}}_k + \sin\theta\,\widetilde{\mathbf{p}}_{kk},$$

and $\mathbf{R}_{kl} \equiv \dfrac{\partial^2 \mathbf{R}}{\partial p_k p_l} = \dfrac{p_k\sin\theta}{\theta}(\widetilde{\mathbf{p}}_l\widetilde{\mathbf{p}} + \widetilde{\mathbf{p}}\widetilde{\mathbf{p}}_l) + (\dfrac{p_kp_l\cos\theta}{\theta^2} - \dfrac{p_kp_l\sin\theta}{\theta^3})\widetilde{\mathbf{p}}^2 + \dfrac{p_l\sin\theta}{\theta}(\widetilde{\mathbf{p}}_k\widetilde{\mathbf{p}} + \widetilde{\mathbf{p}}\widetilde{\mathbf{p}}_k)$

$$+\ (1-\cos\theta)(\widetilde{\mathbf{p}}_{kl}\widetilde{\mathbf{p}} + \widetilde{\mathbf{p}}_k\widetilde{\mathbf{p}}_l + \widetilde{\mathbf{p}}_l\widetilde{\mathbf{p}}_k + \widetilde{\mathbf{p}}\widetilde{\mathbf{p}}_{kl}) - (\frac{p_kp_l\sin\theta}{\theta^2} + \frac{p_kp_l\cos\theta}{\theta^3})\widetilde{\mathbf{p}} + \frac{p_k\cos\theta}{\theta}\widetilde{\mathbf{p}}_l + \frac{p_l\cos\theta}{\theta}\widetilde{\mathbf{p}}_k + \sin\theta\,\widetilde{\mathbf{p}}_{kl}.$$

Denote positions in the body-fixed frame by superscript 0. For rigid bodies I and J with sites i and j defining site-site isotropic potentials U_{ij}^{IJ} the potential energy is

$$U = \sum_I \sum_{J<I} \sum_{i\in I} \sum_{j\in J} f_{ij}(r_{ij}), \qquad \text{where} \qquad r_{ij} = |\mathbf{r}_{ij}| = |\mathbf{r}_i - \mathbf{r}_j| \qquad \text{and} \qquad f_{ij} \equiv U_{ij}^{IJ} \qquad \text{so that}$$

$$\frac{\partial U}{\partial \zeta} = \sum_{J\neq I}\sum_{i\in I}\sum_{j\in J} f'_{ij}(r_{ij})\frac{\partial r_{ij}}{\partial \zeta}, \quad \text{where} \quad f'_{ij} = \frac{df_{ij}(r_{ij})}{dr_{ij}}, \quad \frac{\partial r_{ij}}{\partial \mathbf{r}^I} = \hat{\mathbf{r}}_{ij}, \quad \frac{\partial r_{ij}}{\partial p_k^I} = \hat{\mathbf{r}}_{ij}\cdot\frac{\partial \mathbf{r}_{ij}}{\partial p_k^I} = \hat{\mathbf{r}}_{ij}\cdot(\mathbf{R}_k^I\mathbf{r}_i^0), \quad \mathbf{r}_{ij} = \mathbf{r}^I + \mathbf{R}^I\mathbf{r}_i^0 - \mathbf{r}^J - \mathbf{R}^J\mathbf{r}_j^0.$$

$$\frac{\partial^2 U_{ij}^{IJ}}{\partial r_k^I \partial r_l^J} = f_2(r_{ij})r_{ij,k}r_{ij,l}\epsilon_{IJ} + f_1(r_{ij})\delta_{kl}\epsilon_{IJ},$$

$$\frac{\partial^2 U_{ij}^{IJ}}{\partial p_k^I \partial p_l^J} = f_2(r_{ij})(\mathbf{r}_{ij}\cdot\mathbf{R}_k^I\mathbf{r}_i^0)(\mathbf{r}_{ij}\cdot\mathbf{R}_l^I\mathbf{r}_i^0)\delta_{IJ} - f_2(r_{ij})(\mathbf{r}_{ij}\cdot\mathbf{R}_k^I\mathbf{r}_i^0)(\mathbf{r}_{ij}\cdot\mathbf{R}_l^J\mathbf{r}_j^0)(1-\delta_{IJ}) + f_1(r_{ij})(\mathbf{R}_k^I\mathbf{r}_i^0)\cdot(\mathbf{R}_l^I\mathbf{r}_i^0)\delta_{IJ}$$
$$-f_1(r_{ij})(\mathbf{R}_k^I\mathbf{r}_i^0)\cdot(\mathbf{R}_l^J\mathbf{r}_j^0)(1-\delta_{IJ}) + f_1(r_{ij})(\mathbf{r}_{ij}\cdot\mathbf{R}_{kl}^I\mathbf{r}_i^0)\delta_{IJ},$$

$$\frac{\partial^2 U_{ij}^{IJ}}{\partial r_k^I \partial p_l^J} = f_2(r_{ij})(\mathbf{r}_{ij}\cdot\mathbf{R}_l^I\mathbf{r}_i^0)r_{ij,k}\delta_{IJ} - f_2(r_{ij})(\mathbf{r}_{ij}\cdot\mathbf{R}_l^J\mathbf{r}_j^0)r_{ij,k}(1-\delta_{IJ}) + f_1(r_{ij})[\mathbf{R}_k^I\mathbf{r}_i^0]_l\delta_{IJ} - f_1(r_{ij})[\mathbf{R}_l^J\mathbf{r}_j^0]_l(1-\delta_{IJ}).$$

where $f_1(r_{ij}) = f'_{ij}(r_{ij})/r_{ij}$, $f_2(r_{ij}) = f'_1(r_{ij})/r_{ij}$, $\epsilon_{IJ} = 1$ for $I = J$ and $\epsilon_{IJ} = -1$ for $I \neq J$, and δ_{IJ} is the Kronecker delta.

Self-Assembly of Icosahedral Shells (*PCCP*, **11**, 2098-2104, 2009)

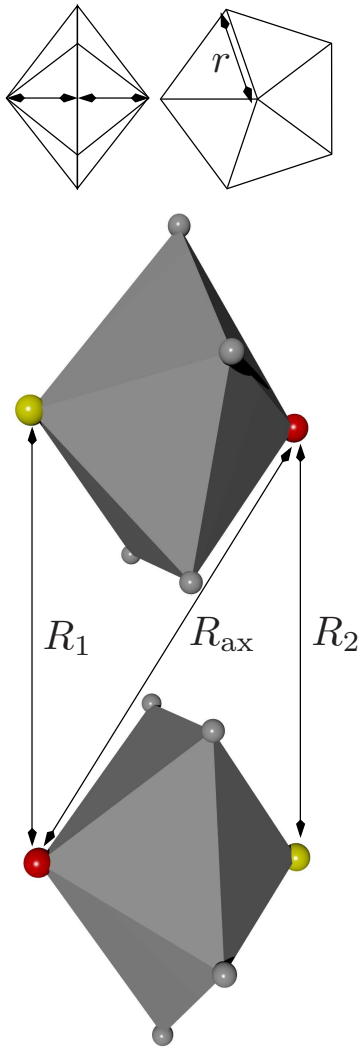

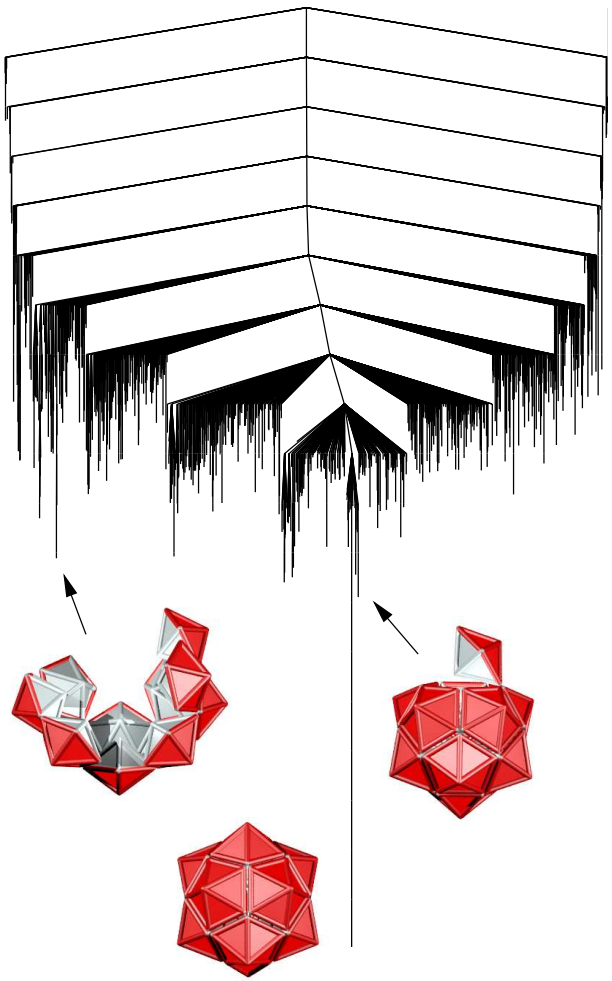

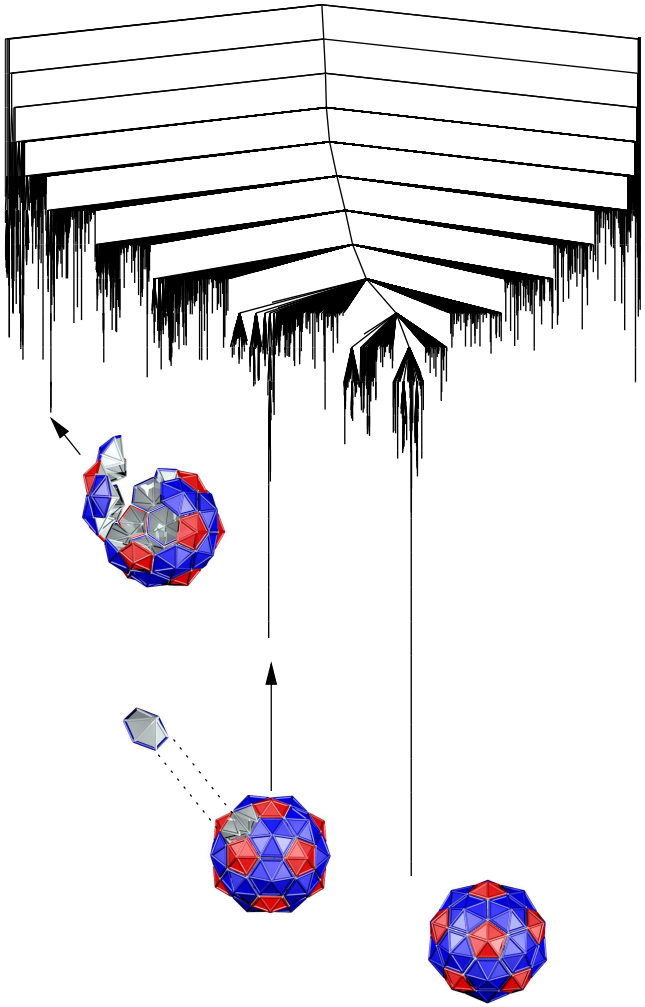

Palm tree disconnectivity graphs with I_h global minima are found for $T = 1$ and $T = 3$ shells constructed from pentagonal and hexagonal pyramids. Landscapes of this form are associated with good structure-seekers.

Emergent Behaviour from Simple Models (*ACS Nano*, **4**, 219, 2010)

Adding two repulsive axial Lennard-Jones sites to an ellipsoidal core produces remarkably versatile building blocks. Oblate ellipsoids favour shells, while stronger repulsion for the longer semiaxis produces tubes and spirals.

Global minima for the oblate ellipsoids include icosahedra for $N = 12$, 32 and 72 ($T = 1, 3$ and 7), the snub cube observed for polyoma virus capsids at $N = 24$, and conical, biaxial, prolate, and oblate shells at other sizes.

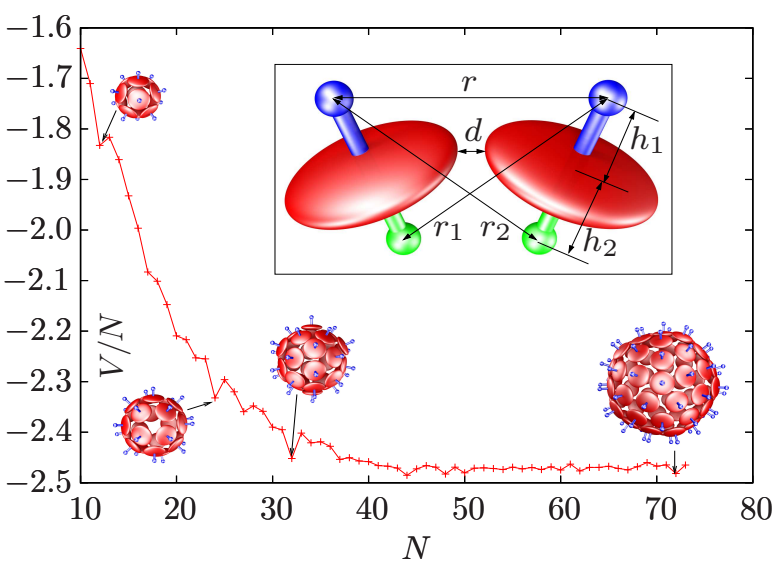

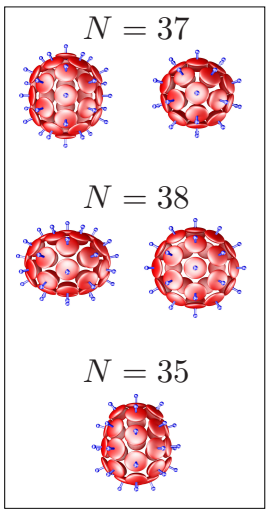

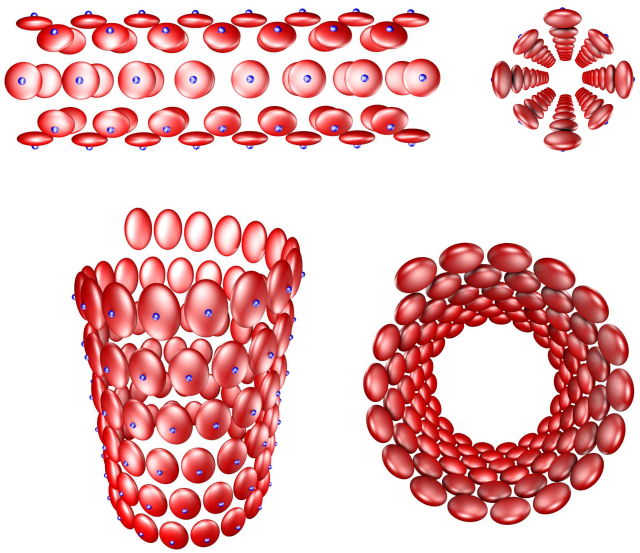

Modelling Mesoscopic Structures (*ACS Nano*, **4**, 219, 2010)

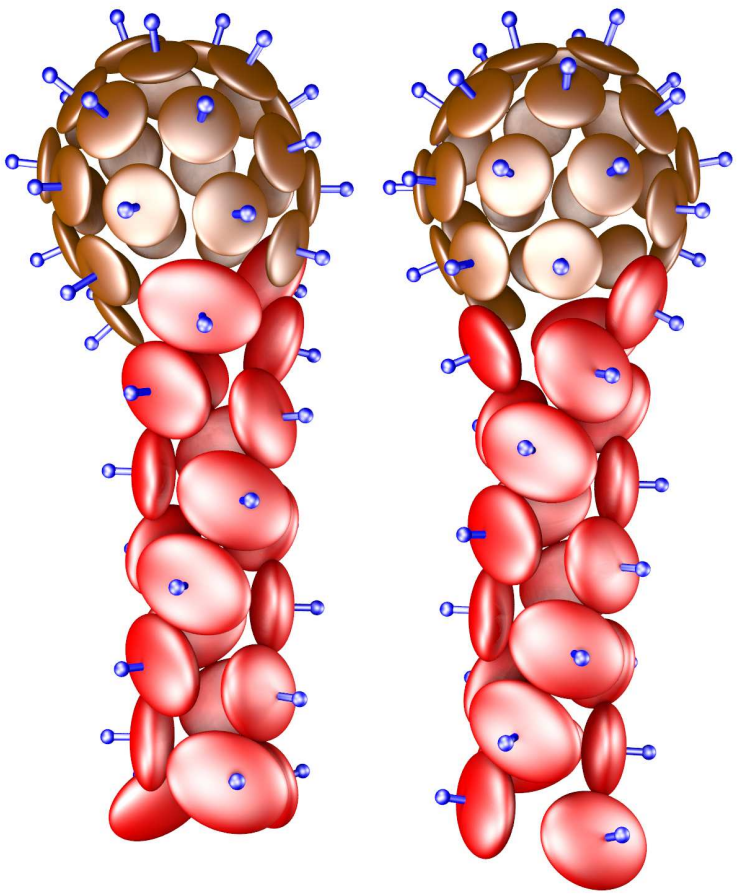

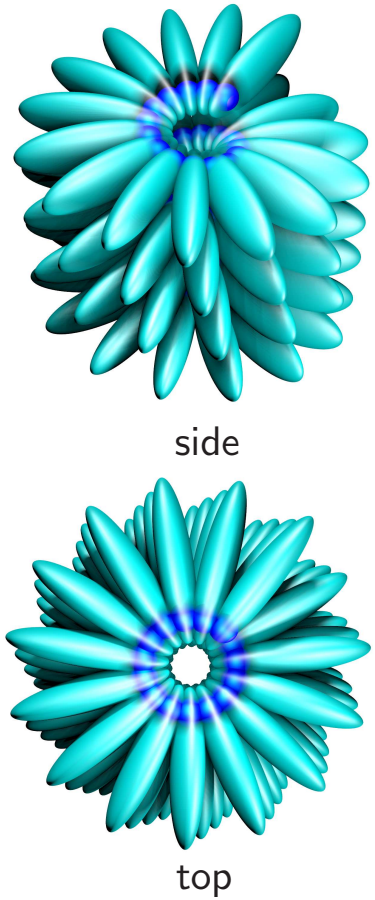

Mixing ellipsoidal building blocks that favour shells and tubes produces structures with distinct head and tail regions (left): the Frankenphage.

Particles with a Lennard-Jones site buried in the ellipsoid assemble into a spiral structure (right) with parameters similar to tobacco mosaic virus.

Nanodevices (*Soft Matter*, **7**, 2325, 2011)

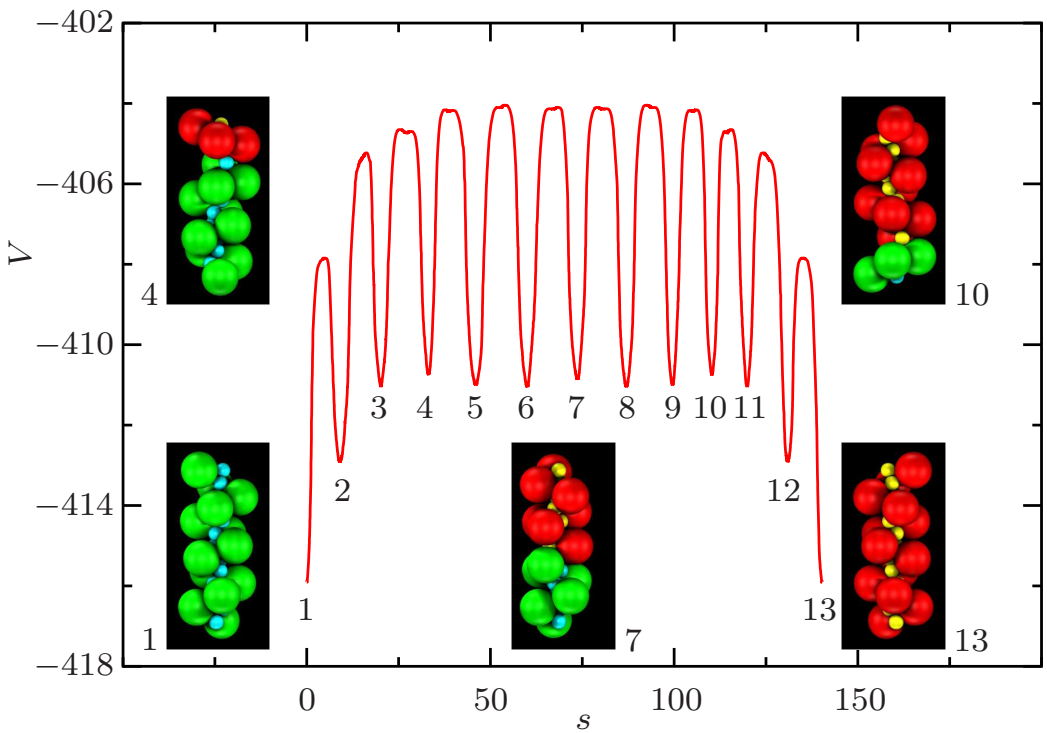

Coupled linear and rotary motion has been characterised for a helix composed of 13 asymmetric dipolar dumbbells in the presence of an electric field.

The helix changes handedness as the boundary between segments propagates along the strand via successive steps that switch the dumbbells.

Connecting Dynamics and Thermodynamics (*Science*, **293**, 2067, 2001)

The organisation of a PES is governed by its stationary points, where Taylor expansions provide local descriptions in terms of Hessian matrices.

The organisation of families of PES's as a function of parameters in the potential is determined by the stationary points that possess additional zero Hessian eigenvalues, known as non-Morse points.

Catastrophe theory provides a local representation of the PES around non-Morse points as a function of both atomic coordinates and parameters.

The splitting lemma reduces the dimensionality to the essential variables, while transversality guarantees that the resulting classifications are universal.

The simplest one-parameter catastrophes are the fold, $f(x) = \frac{1}{3}x^3 + ax$, and the symmetrical cusp, $f(x) = \frac{1}{4}x^4 + \frac{1}{2}ax^2$.

Geometries of the fold and cusp catastrophes.

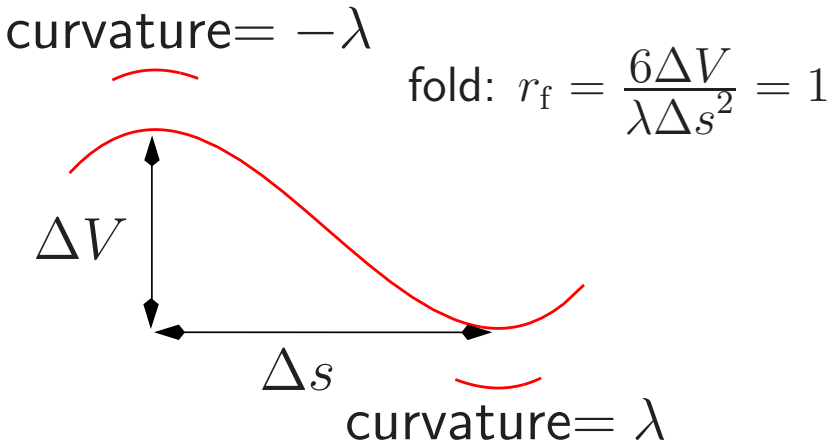

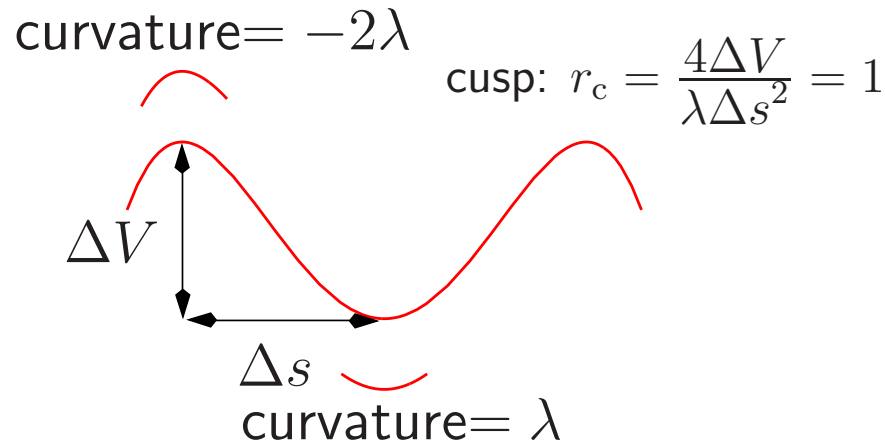

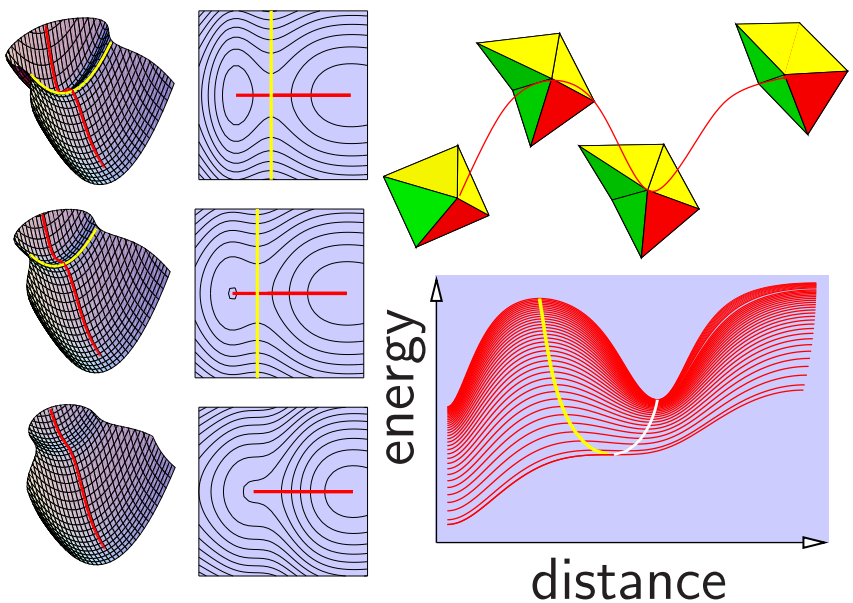

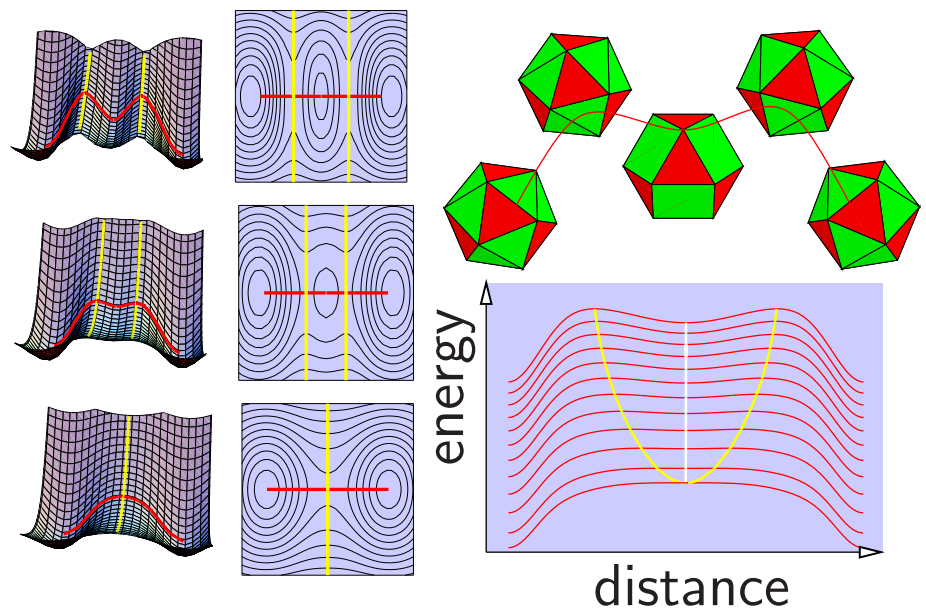

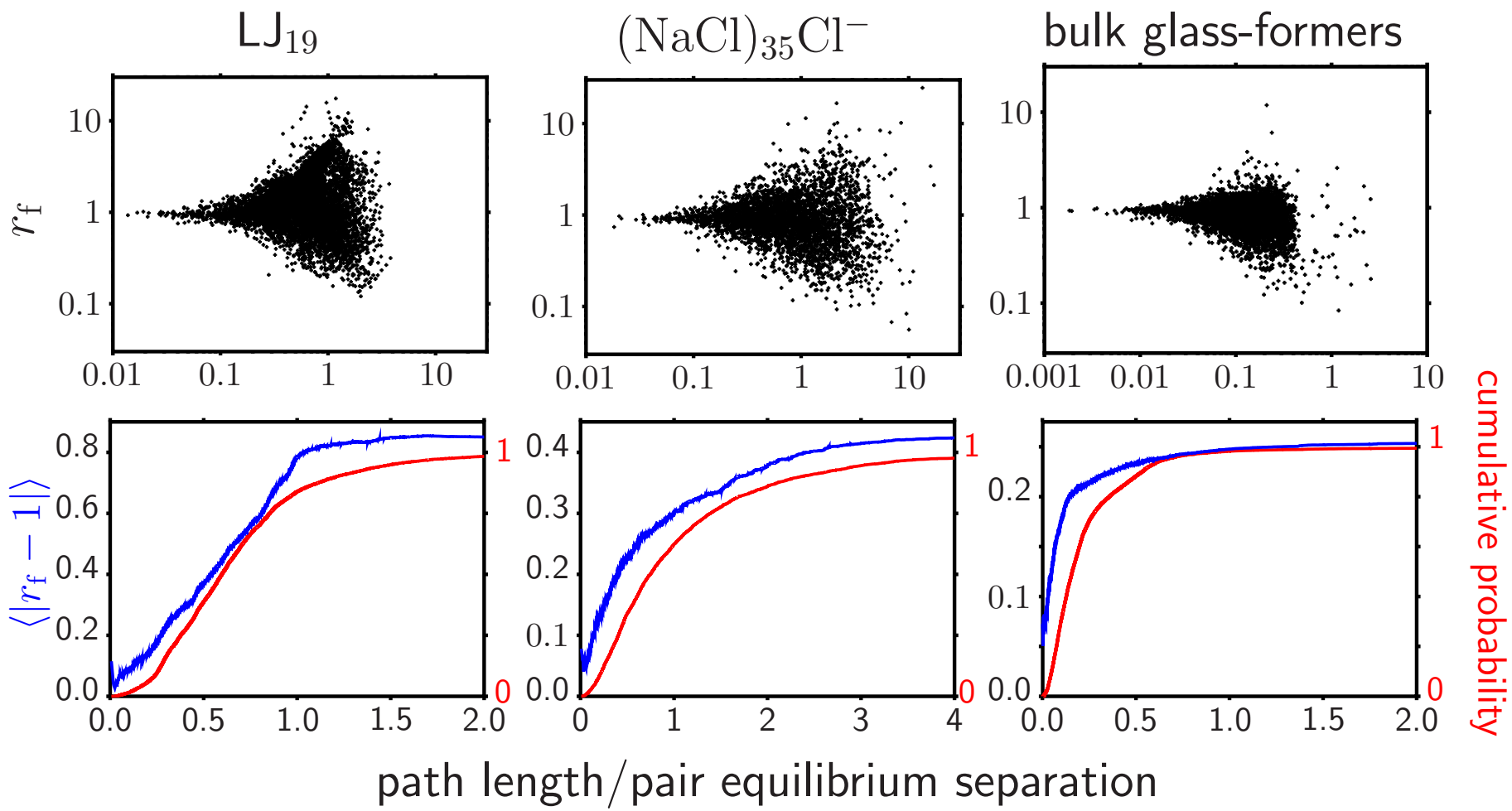

For systems with a fixed potential we effectively have a snap-shot of parameter space. On average, r_{f} remains close to unity for many pathways in both model clusters and bulk, providing an explanation for Hammond's postulate.